Numerical modelling of the nonlinear mechanical behavior of multilayer geosynthetic system for piggyback landfill expansions

http://dx.doi.org/10.1016/j.geotexmem.2016.07.004

PUBLISHER

© Elsevier

VERSION

AM (Accepted Manuscript)

Numerical modelling of the nonlinear mechanical behavior of multilayer geosynthetic system for piggyback landfill expansions

Corresponding author:

Tano, Francis[a,b,c] - francis.tano@ecogeos.fr, francis.tano@irstea.fr / +33140966236, +33628359759

Co-authors:

Dias, Daniel[d] - daniel.dias@ujf-grenoble.fr / +33476827931

Fowmes, Gary John[e] - G.J.Fowmes@lboro.ac.uk / +441509223775

Olivier, Franck[b] - franck.olivier@ecogeos.fr / +33321155570

Stoltz, Guillaume[a] - guillaume.stoltz@irstea.fr / +33140966048

Touze-Foltz, Nathalie[a] - nathalie.touze@irstea.fr / +33140966039

Organization:

[a] Irstea Antony, 1, rue Pierre-Gilles de Gennes 92761 Antony, France

[b] Ecogeos, 5, rue du jeu de Paume, 62000 Arras, France

[c] Lthe, Grenoble Alpes University, OSUG B, Domaine universitaire, BP 53, 38041 Grenoble cedex 09, France

[d] 3SR, Polytech Grenoble Alpes University, Domaine Universitaire BP 53, 38041 Grenoble 09 Cedex 09 , France

[e] CBE, Loughborough University, Leicestershire LE11 3TU, UK

ABSTRACT

Numerical modelling techniques have been increasingly used to assess the integrity of engineering works, such as landfills, that involve interactions between multiple geosynthetics (GSYs). In piggyback landfill expansions (PBLEs), where a new landfill is built over an older one, such interactions are particularly important because multiple GSYs, natural materials, and waste interact with each over. To obtain reliable numerical results, the real mechanical behavior of the GSYs and of the interfaces between GSYs must be considered. Designers, however, often use simplistic assumptions without further analyzing the implications of these assumptions on the results. Such simplifications mainly concern the nonlinear axial stiffness of GSYs, the strain softening at interfaces between GSYs, and the difference between the compressive and tensile behavior of GSYs. By, considering these key aspects, the present study aims to understand the extent to which the results of numerical calculations can be influenced both by the differing compressive and tensile behavior of GSYs and by the assumption of strain softening at interfaces between GSYs. For this purpose, several numerical models are implemented by using the finite-difference code FLAC 2D on a typical PBLE that involves four GSYs and six interfaces. The present work also applies comprehensive, state-of-the-art numerical modelling to study the interactions between multiple layers of GSYs. This study also investigates the nonlinear axial stiffness of GSYs through a series of uniaxial tensile tests. The numerical results show that, if the GSY axial compressive and tensile characteristics are the same, then tensile force is minimized, which induces significant compressive force in the GSYs. The results also indicate that

neglecting strain softening at the interface between GSYs affects interface shear stresses, displacements of GSYs at the interface, and the GSY force distribution, potentially rendering the model unrealistic. Including strain softening, however, allows the assessment (location) of unstable areas along the interface where large displacements occur.

Keywords: Geosynthetics, numerical modelling, interface strain softening, nonlinear stiffness

1. INTRODUCTION AND BACKGROUND

Landfills are increasingly becoming technical-engineering constructions in which waste, various geosynthetics (GSYs), and natural materials (clay, sand, gravel) interact within the lining system (Tano and Olivier, 2014). In a piggyback landfill expansion (PBLE), where a new landfill is built over an older one, these interactions are particularly important because they control the shear stress at the interfaces between GSYs and their deformation and thereby determine the integrity of the lining system.

To assess the performance of a PBLE and the integrity of its lining system, the conventional engineering-design practice is to use the equilibrium-limit approach (Giroud, 1989, Koerner and Hwu, 1991). This method often does not consider some key points, such as staged construction, the multiple interactions between GSYs, and whether stresses are compatible with strains and displacements (Villard et al., 1999). In contrast, numerical modelling techniques can consider these aspects but should also simulate local instabilities and compute stress and strain fields.

For the more rigorous numerical analysis that is required as landfill construction progresses, the real mechanical behavior of the GSYs and the interactions that occur at their interfaces must be considered. This requires modelling all GSY interfaces in the lining system [which is called criterion 1 (CR1)], the staged construction or evolution of the waste properties with depth or stress (CR2), the strain softening at the interface between GSYs (CR3), the difference between the compressive and tensile behavior of the GSY (CR4), and the nonlinear axial stiffness of the GSY (CR5). Even if these five key criteria have been discussed by many authors, they are not always considered in numerical modelling.

The present work comprehensively reviews some twenty-five studies that reflect the current practices used to numerically model interactions between GSYs. These studies are classified in chronological order in Table 1 and are discussed below.

- **Criterion 1: Number of GSY interfaces in model**

In sanitary landfills, the drainage and lining system involves at least two GSYs. These are typically a geomembrane (GMB) overlaid by a protection geotextile (GTX). In many countries (e.g., France), a geosynthetic clay liner (GCL) is often installed beneath the GMB to reduce the thickness of the in-situ sealing clay. In the context of a PBLE, this composite system is often completed with a reinforcement geogrid (GGR) in the PBLE (Tano et al., 2015).Therefore, for the model to represent a realistic situation, the interactions between the multiple GSYs should be considered. If the model does not consider the multiple interfaces between GSY layers, it cannot determine the axial force and strain within the GSY.

Table 1 shows that most previous studies considered less than three GSYs. Among the studies reviewed, only the works of Long et al. (1995) and Chen et al. (2009a) considered the interactions between three GSYs. However, Long et al. (1995) used springs to model all GSYs (GTX, geonet, and GMB), soil, waste material, and the interfaces between GSYs. However, using these simple structural elements to represent the entire landfill and its lining system has limitations because the constitutive model does not properly represent the nonlinear behavior of waste, GSYs, and the interfaces. Finally, in the study of Chen et al. (2009a), none of the following four criteria were taken into account.

- **Criterion 2: Staged construction and evolution of waste characteristics with depth or stress**

In landfills, the mechanical properties of waste evolve with depth, confining stress, waste age (i.e., degradation), and the backfilling level (Tchobanoglous et al., 1993, Gourc et al., 2001, Haque, 2007, Castelli and Maugeri, 2008, Singh and Fleming, 2008). As can be seen in Table 1, most authors to date have considered staged construction. However, only Arab et al. (2011a) clearly considered how waste properties evolve with depth or stress. The authors divided the waste mass into three layers with differing mechanical parameters. However, the mechanical parameters did not evolve gradually with depth; instead, each layer had its own uniform mechanical parameters.

- **Criterion 3: Strain softening at interfaces between GSYs**

Previous laboratory and field studies have revealed that mobilized shear strength often varies along the interfaces between GSYs in such a way that strain is softened at the interfaces. The strain softening reflects the fact that the shear strength gradually increases to a maximum value (peak) before decreasing to a constant value (residual). This nonlinear stress-strain behavior at GSY interfaces was already discussed by several authors (Jones and Dixon, 2005) and was confirmed by several shear tests (Girard et al., 1990, Stark et al., 1996, Izgin and Wasti, 1998, Dixon et al., 2006, Fleming et al., 2006, Fowmes, 2007, Le Hello, 2007, Fowmes et al., 2008, Palmeira, 2009, Eid, 2011, Tanchaisawat, 2013).

Strain softening at interfaces was touched on in most works that appear in Table 1.

Byrne (1994), Reddy et al. (1996), Jones and Dixon (2005), Seed et al. (1988), Filz et al. (2001), and Connell (2002) all considered strain softening at interfaces but did not consider multiple interfaces and GSY; thus, they could not calculate the strains and forces in the GSYs. In contrast, Villard et al. (1999), Haque (2007), Wu et al. (2008), Chen et al. (2009a), and others did not consider strain softening at interfaces but used a single, constant friction angle (peak or residual). Note also that strain softening at interfaces is not included in conventional numerical modelling software. Other software, such as Geostress, Sage Crisp 2D, and FLAC 2D allow it but may require specific code to be developed. Given the relevance of strain-softening behavior at interfaces, it will be discussed in more detail in Section 5.2.

- **Criterion 4: Differentiation between the GSY compressive and tensile behavior**

To simulate the flexibility of GSYs (i.e., the membrane effect) in numerical models, zero inertia is often assigned to the structural elements that represent the GSY. With zero inertia, the GSY operates without bending resistance. Furthermore, unconfined GSYs do not sustain axial compressive force; however, under high confining stress, the axial compressive behavior is not well known. GSYs may be expected to become stiffer under compression with high confining stress. Conversely, given the folds and wrinkles that are often observed on the cover at the foot of the slope (low confinement) of some sites, GSYs are generally considered to sustain zero or very little compressive force. Moreover, although the axial tensile behavior of GSYs can be evaluated from standardized tests [NF EN ISO 10319 (AFNOR, 2008), NF EN 12311-2 (AFNOR, 2013)], the authors know of no standardized test with which to assess the axial compressive behavior of GSYs.

Given this situation, to model the behavior of GSYs, researchers and engineers are forced to make significant assumptions about the GSY compressive characteristic (modulus). By default, simulation software accepts different GSY compressive and tensile behavior, so only one of five studies reviewed herein considered this question. To consider this aspect, two approaches are generally used: First, the compressive modulus is arbitrarily assumed to be one to two orders of magnitude less than the tensile elastic modulus. This approach was used by Fowmes et al. (2008) (1/10), Villard et al. (1999) (1/10 for a GMB and 1/20 for a GTX), and He et al. (2006) (1/100). The second alternative is to consider a compressive strength of zero, such as Long et al. (1995). For the other studies, the axial tensile behavior of the GSY is assumed to be similar to the compressive behavior. In this case, the compressive forces and strains obtained by simulation may be unrealistic (Sia and Dixon, 2012).

Thus, if GSYs are considered to sustain little or no compressive force under confinement or because of possible GSY wrinkles, a robust and accurate model must be developed. To this end, this report presents a detailed parametric study that highlights the main differences between the three current modelling methods based on (i) an unaltered compressive modulus, (ii) an altered compressive modulus, and (iii) zero compressive strength. The details of this study are given in Section 5.1

- **Criterion 5: Nonlinear axial stiffness of GSYs**

When a GSY is subjected to a tensile load, it gradually lengthens with a deformation that depends on its stiffness over time. Thus, GSY stiffness directly determines the force and strain that develop within the material.

As can be seen in Table 1, the nonlinear axial stiffness of GSYs is the least-considered criterion. This is probably because, first, most software does not by default allow this feature to be considered (as in CR3 and CR4) and, second, the authors preferred to use the simplifying assumption of a constant axial stiffness. This is the case, for example, of Sia and Dixon (2012) and Zamara et al. (2014), who used the secant stiffness at yield and at 5% strain, respectively. From among the studies reviewed, only Long et al. (1995) considered how the GSY axial stiffness evolves with strain. This particular feature is further discussed in Section 3.3.

Overall, because CR1 and CR2 depend on the site characteristics (i.e., the number of GSYs and the phases of construction), only CR3, CR4, and CR5 are investigated herein, as discussed previously. Interactions between multiple layers of GSYs (CR1) and staged construction (CR2) are also considered by default. Thus, this study takes into account the nonlinear tensile stiffness of GSYs to compare several numerical simulations of realistic conditions taken from typical

PBLEs. After a detailed description of the case study and material properties, the differentiation between the compressive and tensile behavior of GSYs is investigated in terms of the simulated tensile and compressive forces within a GSY. Furthermore, based on the results of the previous simulations, we also highlight how strain softening at interfaces affects the shear stress at the interfaces, the displacements of GSYs, and the distribution of force within the GSYs.

2. NUMERICAL MODEL

2.1 General description of model

The model is based on realistic conditions and consists of a mixed PBLE with an existing 20-m-high waste cell and a proposed, 20-m-high vertical extension. The entire PBLE sits on a 400-m-long section of in situ stiff clay.

Figure 1 shows a schematic diagram of the model used in this study, which includes two types of materials: The first is municipal solid waste (MSW) contained in the landfill. The MSW is subdivided into old and new waste, corresponding to the existing cell and the new cell, respectively. The second type of material is soil material consisting of the in situ clay on which the PBLE is established and a 1-m-thick sand bed that serves as the subgrade for the new waste. For the new waste, the entire draining and lining system is incorporated into the model. From bottom to the top, this system consists of a GGR within a 1-m-thick subgrade, a GCL, a GMB and a protective nonwoven GTX. The interaction between the materials and the GSY is modelled by six interfaces of zero thickness. The first interface, I1, represents the interface between the

GTX and a drainage gravel layer (not modelled in this study) under the new waste. The second interface, I2, represents the interaction between the above GTX and the GMB. Like I2, the third interface, I3, represents the interaction between two GSYs; namely, the GMB and the GCL. The fourth interface, I4, represents the interaction between the GCL in the draining and lining system and the subgrade layer on top of the existing cell. The two last interfaces, I5 and I6, separate the GGR from the sand layers that are above and below it, respectively.

2.2 Configuration of numerical model

The numerical model was implemented with the two-dimensional (2D) finite-difference modelling code Fast Lagrangian Analysis from Continua (FLAC 2D). Most of the authors [(Byrne (1994), Connell (2002), Jones and Dixon (2005), Fowmes et al. (2005a), Chen et al. (2009b), Zhu et al. (2009) andZamara et al. (2014)] used this code to assess the interactions at the interfaces between multiple layers of GSYs and its large strain capabilities. The software can model forces and strains within multiple layers of GSYs constructed over several stages. In addition, the software can use a nonlinear stress-strain law to model materials, structural elements, and interfaces. The following sections detail the numerical configuration retained for this study.

2.2.1 Mesh and boundary conditions

The PBLE is modelled by using a rectangular mesh. A two-dimensional model is justified by the fact that the geometry of the PBLE, the boundary conditions, and the loading mode (mechanical stresses) are quite similar in all planes parallel to the strain plane of the PBLE cross section. The mesh chosen for materials (waste and soils) consists of 6400 volume elements (zones), each having a size between 1 m × 1 m and 2 m × 2 m (

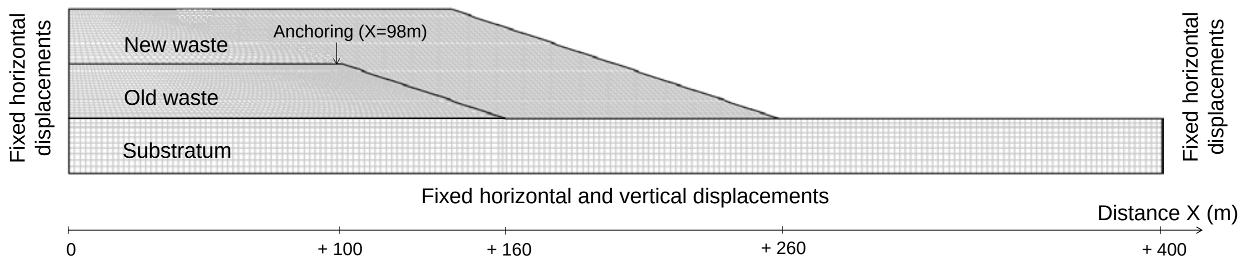

Figure 2). The substratum is modeled by using a coarser 2 m × 2 m mesh that becomes finer as it nears the substratum-waste contact.

At the lower side of the substratum, fixed nodal displacements are imposed because of the assumption that, at this depth, the substratum is stiff enough to not settle under the load of the overlying waste backfill.

At the sides of the model, the horizontal displacements are fixed; the left and right sides of the model are assumed to be sufficiently far (≥100 m) from the crest of the existing waste cell to limit the influence of the boundary conditions.

Moreover, all the GSYs, except the GGR, are fixed (perfect anchoring) on top of the existing waste cell, 2 m from the crest slope (this is generally the case in landfills) at X = 98 m. The GGR was installed with no specific conditions to implement a flat anchor by using the ballast weight of the overlying materials.

2.2.2 Choice and discretization of structural elements

The structural elements were chosen to simulate the GSY behavior described in Figure 3. Thus, the GTX, GMB, and GCL layers in the model are represented by structural beam elements, which can reproduce the membrane effect with zero inertia. These are the only structural elements in FLAC 2D that allow direct interaction between two GSY. Strip elements were used for the GGR. These structural elements are specifically designed in FLAC 2D to simulate the behavior of thin flat reinforcing structures placed within a soil embankment for support. This type of element cannot sustain bending moments and, in addition, the shear behavior at the strip-soil interface is directly defined by a nonlinear shear-failure envelope.

To account for how the GSY axial stiffness changes with strain, each GSY is represented by a concatenation of several structural elements (152 for the GGR and 98 for the others). This allows the properties of each axial beam to vary independently of the other parts of the GSY and as a function of the strain at the given point.

Moreover, to consider strain softening at interfaces, all interfaces are also defined as a concatenation of individual interfaces so that each can move independently. To model the structural elements and interfaces as described previously, two functions were developed in the programming language compiled by the FLAC inbuilt subroutine compiler (FISH).

2.2.3 Phases of model construction

To account for how stress and strain evolve with the backfilling level, six main phases of model construction divided into 15 steps were considered. Phase 1 is the initial equilibrium of the substratum (initialization of gravitational forces); phase 2 is the initialization of node displacements and velocities, then the implementation of the five 4-m-thick layers of old waste. The upper layer is 3 m thick and overlaid with a 1-m-thick sand layer (we assume cover over subgrade). The node displacements and velocities are initialized again during phase 3 before the GGR and its interfaces I5 and I6 are installed in the sand layer. Phase 4 is the installation of the GCL, the GMB, the GTX, and interfaces I2–I4. Next, the first layer of new waste and the first part of interface I1 are implemented in phase 5. Finally, the nine other layers of new waste and the other parts of interface I1 are implemented successively.

3. MATERIALS, GEOSYNTHETICS, AND INTERFACE PROPERTIES

The elasto-plastic Mohr-Coulomb (MC) constitutive model is used to model the soil, the waste material, and the interface behavior. The MC parameters are preferred over the parameters of complex constitutive models such as the creep model. The MC model was used in the majority of the studies mentioned above and is one of the most used in numerical modelling. Thus, the model parameters described in the following section refer to the MC model.

3.1 Mechanical properties of waste

As mentioned previously, this study constructs the model in stages and updates the waste properties depending on the type of waste (old or new) and the depth. Because the backfilling process involves varying the waste properties, a third FISH function was developed to account for them.

The parameter values used for this study are based on the data available in the literature. A detailed description of the parameters for the new and old waste is given below.

3.1.1 Unit weight

Published data on the unit weight of MSW show significant scatter from one site to another (see Table 2) and sometimes within the same site (typically 3 to 15 kN/m^3). The unit weight of MSW depends not only on its composition (percent of plastic, paper, food, etc.) but also on several factors that interact with each other. These are, for example, depth (i.e., effective confining stress), age, and degradation and compaction effort. However, some typical behavior may be identified; for example, the unit weight tends to increase when the waste is degraded (reduction of the void ratio) and the depth increases. This increase in unit weight could have a considerable effect on the stress-deformation behavior of MSW because it influences the stress distribution within the waste (Singh et al., 2009).

This study uses the following hyperbolic law of Zekkos et al. (2006) (Equation 1) which determines the gradual change in unit weight of MSW with depth:

$$\gamma(Z) = \gamma(0) + \frac{Z}{\alpha + \beta Z} \qquad \text{Equation 1}$$

where

α and β : Hyperbolic parameters with α = 3 m^4/kN and β = 0.2 m^3/kN for typical compaction effort and amount of soil;

z : Depth of the layer;

$\gamma(z)$ and $\gamma(0)$: Total unit weight at depth z and near the surface ($z = 0$), respectively.

In this study, the unit weight of new waste is assumed to be less than that of old waste since new waste is fresher and therefore less consolidated than old waste. Based on data from the literature (see Table 2), we use $\gamma(0)$ = 9 kN/m^3 for new waste and $\gamma(0)$ = 10 kN/m^3 for old waste. Moreover, a typical compaction effort and amount of soil are considered for the choice of the hyperbolic parameters α and β . Figure 4 shows the unit weight used in this study as a function of depth.

3.1.2 Elastic parameters: Young’s modulus and Poisson’s ratio

Like the unit weight, the elastic parameters may vary within a given site. For example, Poisson's ratio ν tends to increase as waste degradation increases whereas the elastic modulus could be low for fresh waste. Note also that Young’s modulus E increases with depth and confining stress (Beaven and Powrie, 1995, Castelli and Maugeri, 2008, Singh and Fleming, 2008). Some elastic parameters from the literature are shown in

Table 3, which shows that 0.5 MPa < E < 7 MPa and $0.05 < \nu < 0.45$.
For this study, we assume that the elastic parameters of new waste are less than those of old waste because new waste should be less consolidated and thus more compressible than old waste. Figure 5 shows the profiles of the elastic parameters of the MSW used in this study, which were obtained by using the assumptions just outlined.

3.1.3 Cohesion and friction angle

According to Singh and Murphy (1990) and Jessberger and Kockel (1993), identifying the failure on the stress-strain curve of waste is very difficult. Several authors (Landva and Clark, 1986, Del Greco and Oggeri, 1993, Jessberger and Kockel, 1993, Zekkos et al., 2006) investigated the shear strength of waste and showed that the cohesion c and the friction angle Φ may vary considerably for waste. Table 4 shows this significant scatter, with c ranging from 0 to 85.9 kPa and Φ from 0° to 53°.

Three ranges of c and Φ can be identified: The first set of ranges covers high cohesion (25–100 kPa) and low friction angle (0° to 10°). The second set of ranges is the opposite with low cohesion (0–10 kPa) and high friction angle (25°–40°). The last set of ranges covers the intermediate values. This study uses the second set of ranges because it seems to be most common, based on our experience.

Furthermore, the variation in the shear strength of waste over time can vary considerably from one site to another. This variation depends on several factors, such as composition (plastic, fines, etc.), compaction effort, moisture conditions, age (e.g., degradation), etc. The shear strength (friction and/or cohesion) of waste can increase with time (Carucci et al., 1991, Zhan et al., 2008) presumably as a result of densification. However, the degradation over time can also lower the shear strength of the waste (Turczynski, 1988, Jessberger and Kockel, 1993, Kölsch, 1993, Bray et al., 2009, Varga, 2012).

Since waste placement conditions of old landfills are generally not fully known, a safe-based approach was considered, in which both c and Φ decrease with time. It was also assumed that a modern compaction plant is more efficient than in the past and provides for closer waste fiber intertwining than in the past. A linear decrease of c and Φ over time (with depth) as shown in Figure 6 was thus considered in this study.

3.2 Mechanical properties of soil

The unit weight of soil generally ranges from 12 to 23 kN/m^3 depending on the level of consolidation, organic content, etc. (Linsley et al., 1982, Murthy, 2002). The analysis described herein uses a typical unit weight of 18 kN/m^3 for all soil materials.

For the elastic parameters, the clay substratum should be stiff, as indicated by a Young's modulus of 50 MPa, which was the value used by Jones and Dixon (2005) and Zamara et al. (2014) to model a hard clay substratum. A Young's modulus of 20 MPa is used for the sand layer on top of the existing waste cell, which is the minimum required by the French technical guide GTR 92 for compacted subgrade. A Poisson's ratio of 0.3 typical of normally consolidated soils is assigned to all soil materials. Moreover, because we assume a long-term analysis, a cohesion of 5 kPa and a friction angle of 28° are assigned to the clay. However, the sand subgrade is assumed to have a friction angle of 35° without cohesion. Table 5 summarizes the properties of the waste and soil material.

3.3 Mechanical properties of geosynthetics

The tensile characteristics of several GSY products were assessed according to the standard NF EN ISO 10319 (AFNOR, 2008) for the GTX, GCL, and GGR and according to the standard NF

EN 12311-2 (AFNOR, 2013) for the GMB. For the GMB, for example, uniaxial tensile tests were made on five different 2-mm-thick high-density polyethylene (HDPE) GMBs and on two 1.0-, 1.2-, and 1.5-mm-thick polypropylene (PP) GMBs (GMB a to GMB h; see Figure 7a) at the research and technology platform at the National Research Institute of Science and Technology for the Environment and Agriculture, France.

For numerical modelling, the tensile secant modulus E_ε of the GSY at strain ε is calculated herein as the ratio of the GSY axial stiffness J_ε to the GSY thickness e by using Equation 2

$$E_\varepsilon = \frac{T_\varepsilon}{e.\varepsilon} = \frac{J_\varepsilon}{e} \qquad \text{Equation 2}$$

where

E_ε : Tensile secant modulus at strain ε ;

T_ε :Tensile force on the tensile curve at strain ε ;

J_ε : Secant stiffness at strain ε on the tensile curve;

e : Nominal thickness of the GSY.

The results of the tensile tests show that the axial stiffness and thus the modulus of the GSY are nonlinear. For example, the tensile secant modulus of the HDPE GMB could decrease by a factor of five in going from 2% to 10% strain, as can be seen in Figure 7a. Giroud (1994) also showed that the initial portion of the stress-strain curve of HDPE GMB is nonlinear (Figure 7b) and highlighted that a tensile secant modulus at 2% can be 3.5 times greater than the tensile secant modulus at the yield peak (generally 10% to 12%). This nonlinear behavior of GMBs could be due to their polymeric nature (HDPE, PP) and the way in which they are manufactured. In fact, when a GMB is submitted to a tensile force, a material reorganization may occur, accompanied by a change of the mass per unit area of the fabric. This partial restructuration leads to a change of the axial resistance as strain increases, and thus of the stiffness. For the GTX, GGR, and GCL, the change in axial stiffness is also due to their arrangement and fiber reorganization. Thus, imposing a constant stiffness in numerical modelling may lead to an overestimation or underestimation of the calculated strains. Herein, we allow the GSY modulus to evolve with strain as per the results of tensile tests. For this purpose, a fourth FISH function was developed to update the modulus when a level of strain is reached. Between 0% and 1%, however, a single value was used for the modulus (see Figure 8).

Moreover, for safely analyses, we selected the following four GSYs with the lowest strength:

- an 8-mm-thick nonwoven PP GTX of 1200 g/m² with a tensile strength Rt = 52.5 kN/m at 100% strain;
- a 2-mm-thick HDPE GMB with Rt = 33 kN/m at 12% strain;
- a 7-mm-thick sodium GCL of 5000 g/m² with Rt = 32 kN/m at 38% strain;
- a 2.5-mm-thick uniaxial polyvinyl alcohol (PVA) GGR with Rt = 200 kN/m at 8% strain.

The profiles of the tensile secant modulus of the four GSYs are presented in Figure 8 and Table 6.

3.4 Interface properties

The MC model is used for all interfaces. This model requires the following four parameters: shear stiffness κ_s, normal stiffness κ_n, cohesion c, and friction angle Φ.

3.4.1 Shear and normal interface stiffness

The shear stiffness κ_s defines the slope of the initial part of the curve of shear stress vs displacement and thus directly determines the shear displacements at the interfaces. According to Jones and Dixon (2005), most values of κ_s used to model GTX-GMB interfaces range from 2.4 to 3.8 MPa/m, so a typical value of 3 MPa/m is used herein. Wu et al. (2008) and Zamara et al. (2014) used very similar values for a GTX-soil interface (3.33 MPa/m) and a GTX-GMB interface (4.5 MPa/m), respectively. However, greater values may also be found in the literature, such as 15.9 MPa/m for a GTX-GMB interface (Sia and Dixon, 2012), 24.5 MPa/m for a GSY-GSY interface (Filz et al., 2001), and 49 MPa/m for a GGR-soil interface (Sitharam et al., 2006). Furthermore, Fowmes (2007) conducted a parametric study on the shear stiffness of a textured GMB–nonwoven-GTX interface and showed that a κ_s = 10 MPa leads to a proper stress vs displacement curve.

For the normal stiffness κ_n, an arbitrarily large value is $10\kappa_s$, which is often considered to avoid interpenetration of the nodes during computation.

The present study uses the Itasca (2005) recommendation, which is described in Figure 9.

According to Itasca (2005), a good rule of thumb is to use a maximum κ_s and κ_n of $10\kappa_{eq}$, with κ_{eq} given by Equation 3:

$$K_{eq} = \max \frac{K + \frac{4}{3}G}{\Delta z_{min}} \qquad \text{Equation 3}$$

where

K_{eq}: Apparent and equivalent stiffness;

K and G: Bulk and shear moduli, respectively, of the adjoining zone;

Δz_{min}: Smallest width of an adjoining zone in the normal direction.

Setting K_s and K_n to ten times the soft-side stiffness ensures that the interfaces will minimally influence the system compliance. As per this procedure, we use an initial value of $K_s = 10$ MPa/m, following the Fowmes (2007) parametric study. In the Itasca (2005) procedure, an initial value $K_s < 10K_{eq}$ can be used; otherwise, K_s should be limited to $10K_{eq}$ because a large K_s increases the computation time without significantly affecting the results. In the case study, because $K_s = 10$ MPa/m is less than the calculated $10K_{eq}$ at all interfaces, we use $K_s = 10$ MPa/m at all interfaces. Finally, K_n has been set to $10K_s$ to avoid node interpenetration.

3.4.2 Cohesion and friction angle

The cohesion c and friction angle Φ of GSY interfaces depend on several factors, such as the type of interface (textured, smooth, etc.), the moisture content (wet or dry), the confining pressure, and the shear displacement rate (Criley and Saint John, 1997, Koerner and Koerner, 2001, Stoewahse et al., 2002, McCartney et al., 2004). Table 7, which summarizes 35 c-Φ pairs at the peak and at large displacements (residual), shows that the shear strength of GSY interfaces is generally low. The nonwoven-GTX–GMB interface exhibits the smallest shear strength, with a residual friction angle often below 10°.

For this study, all interfaces are assumed to be wet because of the leachate and the surrounding moisture. Thus, zero cohesion is assigned to all interfaces because the GSY interfaces are assumed to have zero shear resistance when there is no confining pressure.

Concerning interfaces I1 and I4, a peak friction angle of 28° is used based on a gravel-sand friction angle of 35° and a coefficient of interaction (COI) of 0.75. The COI is given by

$$COI = \frac{\tan\Phi_{interface}}{\tan\Phi_{granular\ layer}} \qquad \text{Equation 4}$$

COI = 0.75 is the lowest COI from among several GTX-granular sand interfaces (Myles, 1982). The friction angles of interfaces I2 and I3 are derived from the literature reviewed in Table 7. For interfaces I5 and I6, a peak friction angle of 29° is assigned by assuming $COI = 0.8$, which is consistent with pull-out tests (Bakeer et al., 1998, Yuan, 2002, Liu et al., 2014) and GSY technical data sheets. As discussed above, the strain-softening behavior of interfaces is also considered. A decrease in friction angle by 5° is assumed at all interfaces at 2 and 5 mm relative displacements for GSY-GSY and GSY-soil interfaces, respectively. The peak shear strength of interfaces involving GSYs is reached between 2 and 8 mm of displacement (Stark and Poeppel, 1994, Stark et al., 1996). The peak shear strength of the GSY-GSY interface is rapidly reached near 2 mm of displacement and that of the GSY-soil interface at about 5 mm of displacement (sometimes more). Figure 10 shows the friction angle Φ as a function of interface displacement for the six interfaces. Table 8 gives the values of all interface parameters used in the modelling.

4. METHODOLOGY

The differentiation between the compressive and tensile characteristics of GSYs was investigated by a series of simulations in which the ratio between the tensile modulus (E_tract) and the compressive modulus (E_comp) was decreased. Each simulation is done on the GMB which is the main component of the lining system. To better compare the force, we use the peak friction angle because it leads to overall higher forces within the GMB. The parametric study was done with ten values of E_comp and a compressive strength of zero (Rc = 0 kN). The 10 moduli measured correspond to E_comp = E_tract/X with X varying from 1 to 1000. One simulation was done with E_comp = 0 MPa; for this case, the value 0.1 was used for E_comp instead of 0 to avoid numerical errors and instabilities. A FISH function was developed to change the compressive modulus E_comp when strain becomes compressive. The behavior of the simulated cases is presented schematically in Figure 11.

The analysis consists of comparing the axial compressive and tensile forces calculated within the GMB for each case investigated. Furthermore, to emphasize the main differences that could result when using a constant friction angle and the strain-softening behavior, three cases are simulated. These three cases correspond to a constant peak-friction angle (12°; see Table 8), a constant residual-friction angle (7°; see Table 8), and a friction angle that evolves with the interface displacement (strain softening; see Figure 10). For the strain-softening behavior, updated version of the FISH code developed by Fowmes (2007) and used by Sia and Dixon (2012) and Zamara et al. (2014) was used. This code was modified and optimized to improve the computing speed. The differences between the three cases given above are analyzed in terms of interface shear displacement, shear stress, and also the force or strain within the GMB.

5. RESULTS AND DISCUSSION OF NUMERICAL SIMULATIONS

5.1 Differentiation between compressive and tensile characteristics of geosynthetics

Figure 12 shows the axial tensile and compressive forces calculated for the GMB for each of the ten moduli and for zero compressive strength at two backfilling levels (H = 20 m and 40 m). From this figure, the tensile forces are seen to be nonlinear in E_comp. Moreover, the lowest tensile forces (33.1 kN at H = 40 m) correspond to the two cases E_comp = E_tract and R_comp = 0; they are thus the least-safe cases. At H = 40 m, the difference between these cases and the others reaches 13.9% (≈33 kN versus ~38 kN). The maximum simulated tensile forces are 6.7 kN and 38.4 kN which are reached at H = 20 m and H = 40 m, respectively. They correspond to the cases E_comp = E_tract/100 and E_comp = E_tract/500. Furthermore, for E_comp ranging from 0 to E_tract/50, no other obvious difference appears between the computed tensile force and compressive force.

The decrease in E_comp logically results in a decrease in the calculated compressive forces. Thus, the maximum of the compressive force always occurs for E_comp = E_tract. The minimum compressive force always occurs for R_comp = 0, which systematically gives a calculated compressive force of zero. Moreover, note that, from E_comp = E_tract/2 onwards, the calculated compressive forces decrease sharply below 1 kN when E_comp ≤ E_tract/50.

Therefore, if we assume that GSYs cannot sustain compressive force (or very little) and to account for possible GSY wrinkles, choosing the safest approach (i.e., maximizing the tensile forces) is preferable. Thus, the results of this study indicate that E_comp ≤ E_tract/50 should be used for modelling the difference between the compressive and tensile behavior of GSYs.

Based on this discussion, a compressive modulus E_comp = E_tract/100 appears to be appropriate. Thus, for the comparative study presented in Section 5.2, the compressive modulus of all GSYs is set to one hundredth of their tensile moduli.

5.2 Use of strain softening at interface between GSYs

Figure 13 to Figure 16 compare the main results of the three simulations (i.e., peak-friction angle, residual-friction angle, and strain softening) described in Section 4. Figure 13a shows how the friction angle, which is related to the shear strength, varies along interface I2 for a height of backfilling H = 20 m. At H = 40 m, the residual value is reached along I2 and I3 and excessive displacements larger than 3 m are calculated. At this stage of backfilling, the computed shear displacements are unrealistic because an instability (safety factor <1) is observed. The FLAC calculation cannot converge when failure is reached, which leads to unrealistic calculated displacements.

Focusing on H = 20 m, Figure 13a shows that the friction angle remains constant at 12° and 7° for the peak and residual cases, respectively. When the friction angle is held constant at the peak or residual value, the shear strength of the interface remains constant regardless of the shear stress and displacement. On the contrary, when using strain softening, the friction angle varies along interface I2 and depends on shear displacement. This variation allows the assessment of unstable areas along the interface where large displacements occur. For example, along the slope (between X = 98 m and X = 162 m) and the right-most 64 m of the lower flat area, the friction angle reaches the residual value ($\emptyset = 7°$) because of large displacements. Consequently, shear displacements (Figure 13b) are greater in these zones with a maximum total displacement of 154 cm occurring at the slope and 46 cm at the right-most part of the lower flat area. This high value (154 cm) of shear displacements along interface I2 (GTX-GMB) is associated with a strain level of 15.9% in the GTX around the anchor point.

Note that the results of the residual case are quite similar to those of the strain-softening case for the configurations considered in this study. We attribute this similarity to the fact that, at this stage (H = 20 m), the large shear displacements occur rapidly along a significant portion of interface I2. This pattern was confirmed by Fowmes et al. (2005b), who showed that, when large displacements occur rapidly, the peak friction and the shape of the strain-softening curve have no major impact on the interface behavior, which depends mainly on the residual-friction angle. For the case of peak friction, interface I2 does not move significantly when the shear displacements are limited to 15 cm. This result is due to the greater shear strength of the interface, which can therefore bear more shear stress.

To complete this analysis, the study of Filz et al. (2001) on the Kettleman Hills landfill proves useful because it concerns the case where the interface GTX-GMB failure is progressive and slow. The authors analyzed the effect of the use of the peak-friction angle (11°), the residual-friction angle (6.5°), and the strain softening on the calculated safety factor. The authors showed that the use of the peak-friction angle leads to a 10% underestimate (24.7 m instead of 27.4 m) of the real failure height (27.4 m) while the use of the residual-friction angle leads to a 35% overestimate (36.9 m instead of 27.4 m) of this failure height. The use of the strain-softening behavior however, leads to an accurate description (27.1 m instead of 27.4 m) of the observed failure height with an accuracy of 99% (ratio between the calculated failure height and the observed one).

Figure 14a and Figure 16a show the mobilized shear stress along I2 for H = 20 m and H = 40 m, respectively. These results show that applying the peak-friction-angle approach generally leads to more shear stress because of the larger shear strength. For example for H = 20 m, along the slope (except for the corner at X = 160 m), the shear stress increases up to 37 kPa (75 kPa for H = 40 m) when using the peak-friction-angle whereas it increases to 26 kPa (48 kPa for H = 40 m) when using the residual-friction-angle and strain softening. These calculated shear stresses are due to the overlying waste mass that slips along the slope.

For H = 20 m, the shear stress decreases sharply from almost 40 kPa to less than 5 kPa at the corner (X = 160 m) when using the peak-friction angle. With increasing distance, the shear stress remains less than 5 kPa at the beginning of the lower flat area (from 160 to 180 m) and then increases to 18 kPa at about 220 m. This sharp decrease in shear stress near 160 m can be explained by the fact that interface I2 has high shear strength and so can withstand the shear stress along the upper part of the slope, with the result being a lack of shear stress at the corner at 160 m. For H = 40 m, the shear stress is maintained at a constant level around 75 kPa because of the additional load above H = 20 m. However, when using the residual-friction angle or strain softening, sharp spikes to 68 and 275 kPa for H = 20 m and H = 40 m, respectively, occur in the shear stress at the corner (160 m). For these cases, interface I2 has low shear strength and cannot withstand all the shear stress along the slope from 100 to 160 m, resulting in significant shear stress being concentrated at the corner (shear stress report).

Focusing now on the tensile forces in the GTX at H = 20m as shown in Figure 14b, the main zone subjected to tensile forces appears to be at the top slope (in the following analysis, we use the sign convention whereby negative forces are tensile forces). The GTX slips along the GMB and, because the GTX is anchored at the top slope, it lengthens due to the tensile force that accumulates around the anchorage point. Therefore, high shear displacements along interface I2 will cause significant tensile force to be exerted in the GTX. This is why using the peak-friction angle leads to limited tensile force (less than −2 kN) in the GTX whereas this tensile force reaches −13 kN when using the residual-friction angle or for the strain-softening case; a difference of 550%. In all cases for H = 20 m, this tensile force remains less than the GTX tensile strength (−52.5 kN/m, see Section 3.3). However, for H = 40 m, the tensile force presented in Figure 16b exceeds the tensile strength of the GTX along almost all the slope (from 100 to 136 m) and the first part of the lower flat area (from 160 to 180 m); hence, this would lead to tearing of the GTX because it would slide at the interface between the GTX and the GMB (I2).

Furthermore, upon analyzing, Figure 14c, which shows the spatial distribution of the axial forces in the GMB at H = 20 m, the increase in the mobilized shear stress at the corner at 160 m seems to lead to a large axial tensile force of about −10 kN. Moreover, when using the peak-friction angle, the main zone subjected to tensile force appears to be at the top of the slope (at about 110 m, which is similar to the situation for the GTX), whereas, when using the residual-friction angle or softening, the zone subjected to tensile force spreads all along the downward slope (130 to 160 m) before increasing at the corner (160 m), as already discussed. These differences are probably due to the fact that a more-stable I2 interface (i.e., good adherence between the GTX and the GMB) translates into more stress modes in the GTX (Figure 14b) being transmitted into the GMB. In fact, a large friction angle (i.e., good shear strength) means the slippery overlying waste mass is retained because of significant force around the anchor point, whereas a small friction angle tends to facilitate movement of the overlying waste toward the foot of the slope (i.e., the corner at 160 m) where the shear stress is greater.

Along the slope (except at the corner), the tensile force calculated in the GMB is less than −3 kN when using the residual-friction angle or strain softening, whereas the tensile force reaches −6 kN when using the peak-friction angle; a difference of 100%. Whatever the case, the tensile force in the GMB is not sufficient to tear the GMB because the GMB tensile strength is −33 kN (see Section 3.3). It is essential to note that the low values of the tensile force in the GMB calculated when using the residual-friction angle or strain softening are also related to the friction angle, and thus to relative shear displacements of the interface I3 (GMB-GCL) beneath the GMB. The distribution of the friction angle and the relative shear displacements as a function of distance are presented in Figure 15a and Figure 15b for both I2 (GTX-GMB) and I3, respectively. Due to the fact that the friction angle of I3 is higher than the friction angle of interface I2 along the slope and the lower flat area, the relative shear displacements of I3 (sliding of GMB along GCL) are limited to less than 10 cm while the relative shear displacements of I2 (sliding of GTX along GMB) reach 154 cm. Therefore, the GMB does not slide significantly on the GCL and hence it does not lengthen significantly. For this reason a low value of tensile force, less than −6 kN, is calculated in the GMB.

Finally, increasing the height of backfilling to H = 40 m leads to high tensile forces in the GMB as shown in Figure 16c. The tensile forces are essentially located at the slope top around the anchorage point. The tensile forces reach almost −30 kN for the residual and strain softening cases and exceed the tensile strength of the GMB (−33 kN) when using the peak friction. Because the properties of the GSY interfaces evolve as a function of backfilling and thus with interface displacement, simplifying this strain-softening behavior by using a constant peak- or residual-friction angle could alter the magnitude and distribution of the interface shear displacement and shear stress, force, and strain in the GSY layers. Choosing the proper interface behavior is thus crucial. With the use of the strain-softening behavior, obtaining reliable results from the numerical simulation is possible, and such an approach would also add the possibility of detecting interface areas where instabilities may occur (i.e., large shear displacement when residual-friction angle is attained).

6. SUMMARY AND CONCLUSIONS

Numerical modelling techniques are increasingly used to assess the performance of engineering works involving multilayered geosynthetic (GSY) systems. The present work applies comprehensive, state-of-the-art numerical modelling to study the interactions between multiple layers of GSYs. The results reveal the consequences of the conventional assumptions made regarding the mechanical behavior of both the interfaces and the GSY. These simplifying assumptions involve the strain-softening behavior at GSY interfaces, the nonlinear stiffness of GSYs, and the difference between the compressive and tensile behavior of GSY. To demonstrate that these aspects must be considered, we compare the results of several numerical models that we implemented with finite-difference software. The simulations were configured to represent a typical piggyback landfill expansion based on realistic landfill conditions. The modelled lining system includes four GSYs, which are, from top to bottom, a geotextile (GTX), a geomembrane (GMB), a geosynthetic clay liner (GCL), and a geogrid (GGR). The results of this study lead to the following conclusions:

(1) For the numerical modelling of GSY interaction, when the compressive and tensile characteristics of GSYs are assumed to be the same, the simulated tensile forces are minimized with respect to the case when compressive and tensile behavior is treated as different. Simulations indicate that this underestimation is associated with significant compressive force.

(2) Comparison of several simulations suggest that a compressive modulus two orders of magnitude less than the tensile modulus (E_comp = E_tract/100) is suitable to differentiate between GSY compressive and tensile behavior. This ratio corresponds to the safest approach (i.e., maximizing the tensile forces) either because the GSYs cannot sustain compressive force (or very little) or because it accounts for the possible wrinkles that may occur under compressive force and which is difficult to numerically model with current techniques.

(3) Choosing the peak-friction angle, residual-friction angle, or strain softening for the GSY interface may give different results for the distribution, the magnitude of the tensile force within the GSY system, and the shear stress and displacements at the interfaces. The results obtained herein indicate that high friction angles (i.e., peak) for the interface between GTX and GMB lead to an increasingly mobilized shear stress .For the low friction angle (i.e. residual), the shear stress along the slope is lower but there is a sharp increase at the slope corner. This increase is attributed to the fact that the GTX-GMB interface, which exhibits low shear strength, cannot withstand the shear stress that accumulates along the slope, so the shear stress transfers to the corner and is concentrated there (load transfer).

(4) Due to the fact that interface friction angles may change during construction, the use of the peak friction angle for interfaces may lead to an unsafe design while applying the residual parameters may lead to an unrealistically conservative design when shear displacement is progressive. Moreover, when large interface displacements occur, no distinct difference results from using the residual-friction angle versus using strain softening can be observed.

(5) The results of the numerical simulations also show that, when the GTX-GMB interface exhibits high shear strength, some aspects of the stress modes of the GTX are transmitted to the underlying GMB. Thus, when using a high friction angle (peak, for example), the main zone subjected to tensile force is the top slope for both the GTX and the GMB. For the low-interface shear strength (residual, for example), the main zone subjected to tensile force in the GMB is on the contrary the downward slope when the height of backfilling does not exceed the top slope

altitude. Above this level of backfilling, the main zone subjected to tensile force moves toward the top slope because of the additional load above the top slope.

(6) The results also show that the tensile force in the GTX is mainly due to the fact that it slips along the GMB. Because it is anchored at the top of the slope, it lengthens as tensile force accumulates around the anchorage point. Thus, a GTX-GMB interface with a low shear strength associated with high shear displacement would cause the tear of the GTX by excessive high tensile force.

(7) Finally in landfills, the tensile force developed in the GMB appears to be directly related both to the shear strength of the upper GTX-GMB interface and to the lower GMB-GCL interface. A high friction angle of the lower interface would help to limit the tensile force in the GMB while a high friction angle of the upper interface would increase the tensile force. The reverse of this observation is also true.

7. AKNOWLEDGMENTS

Special thanks are due to J. Bruhier at Huesker France for the productive discussions and for providing us with technical data on their geogrid (GGR), geotextile (GTX), and geosynthetic clay liner (GCL) products. We also thank AfitexFrance (GTX), Fibertex France (GTX), Maccaferri France (GGR), and SKZ Germany (GTX, GCL) for the technical data sheets and the associated tensile tests. Finally, we are grateful to D. Croissant at IRSTEA Antony, France and to P. Mailler at IFTH, France for the tensile tests conducted on GMB and GTX products, respectively.

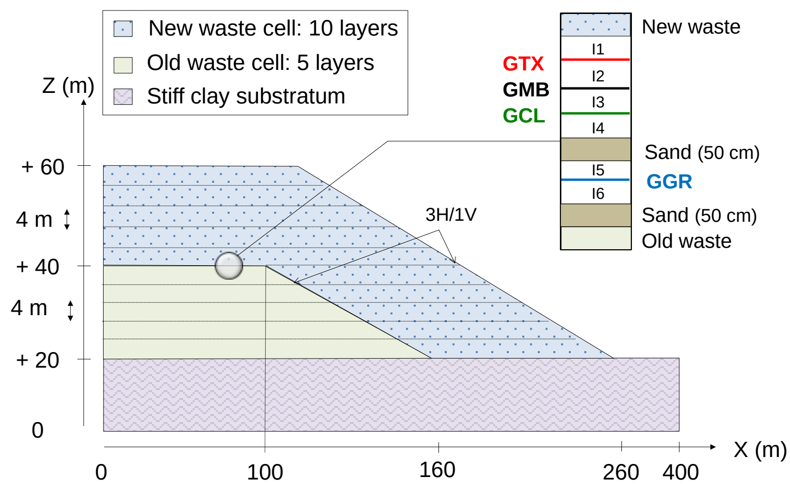

Figure 1. Simplified diagram of the model of piggyback landfill expansion used for the simulations. The labels I*x* in the legend refer to the interfaces between the various materials.

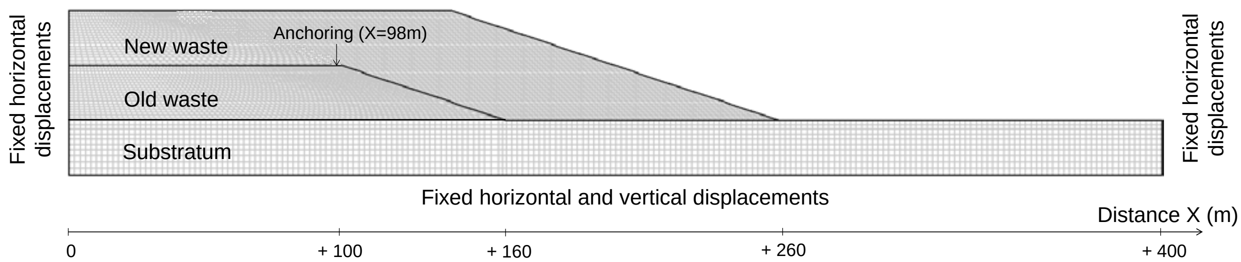

Figure 2. Finite-difference mesh for numerical model.

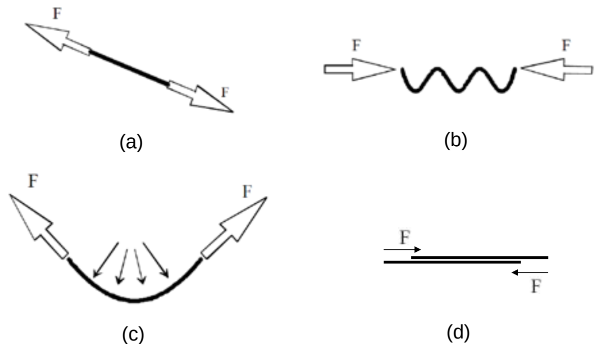

Figure 3. Main behavior of tensile and compressive modes of a GSY: (a) extension due to tensile force, (b) wrinkles due to compressive force, (c) membrane effect due to bending force (Villard et al., 2002), (d) interface sliding due to shear force.

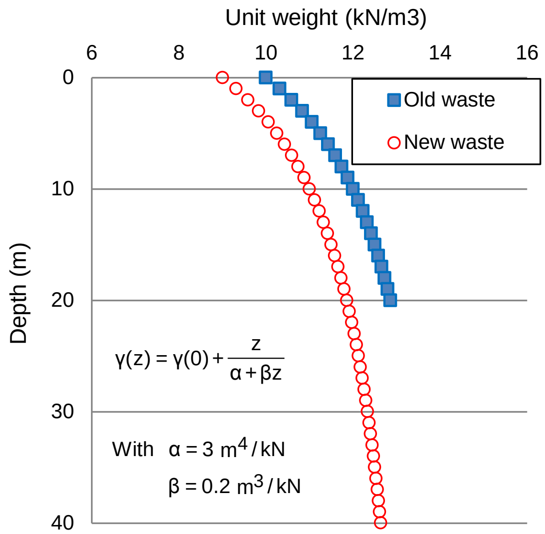

Figure 4. Depth as a function of unit weight for new waste and old waste used in this study.

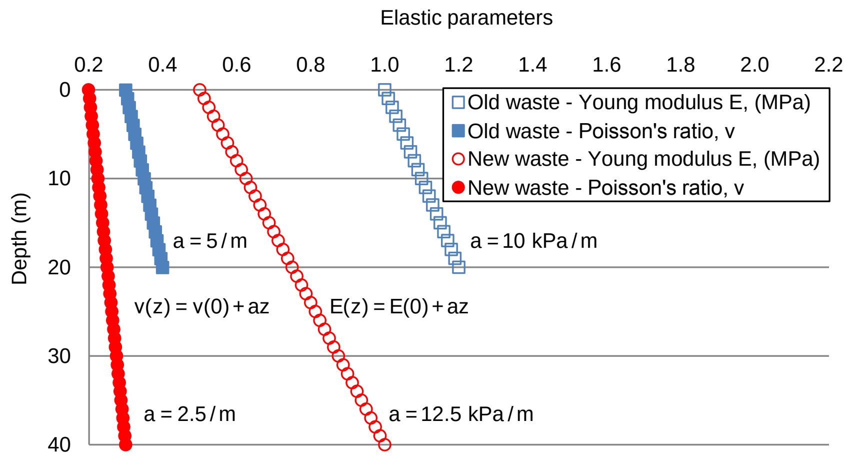

Figure 5. Depth as a function of elastic parameters for new waste and old waste used in this study.

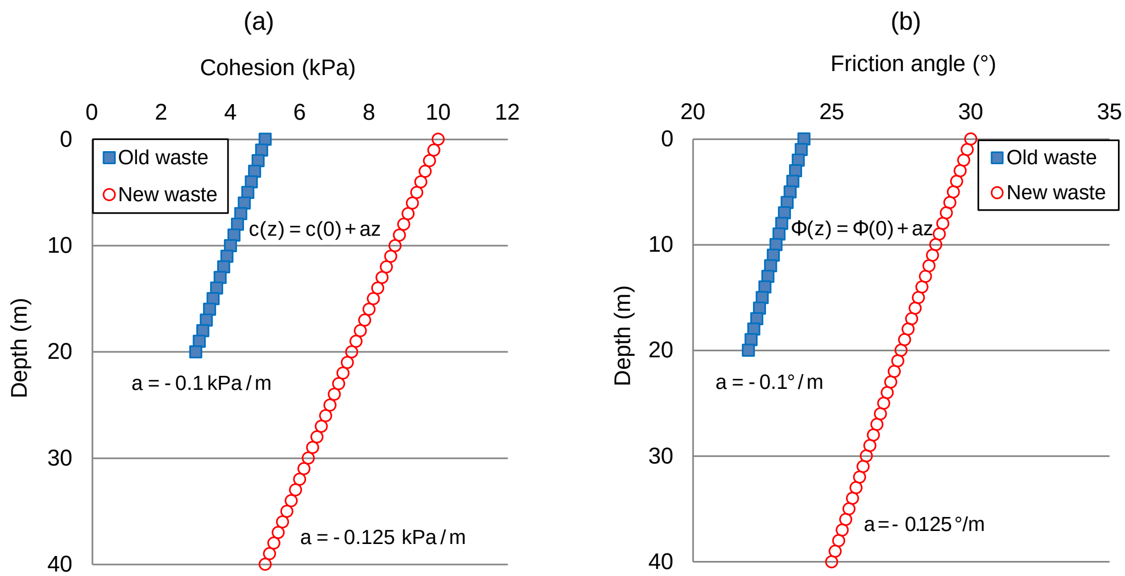

Figure 6. Depth as a function of (a) cohesion and (b) friction angle for new waste and old waste used in this study.

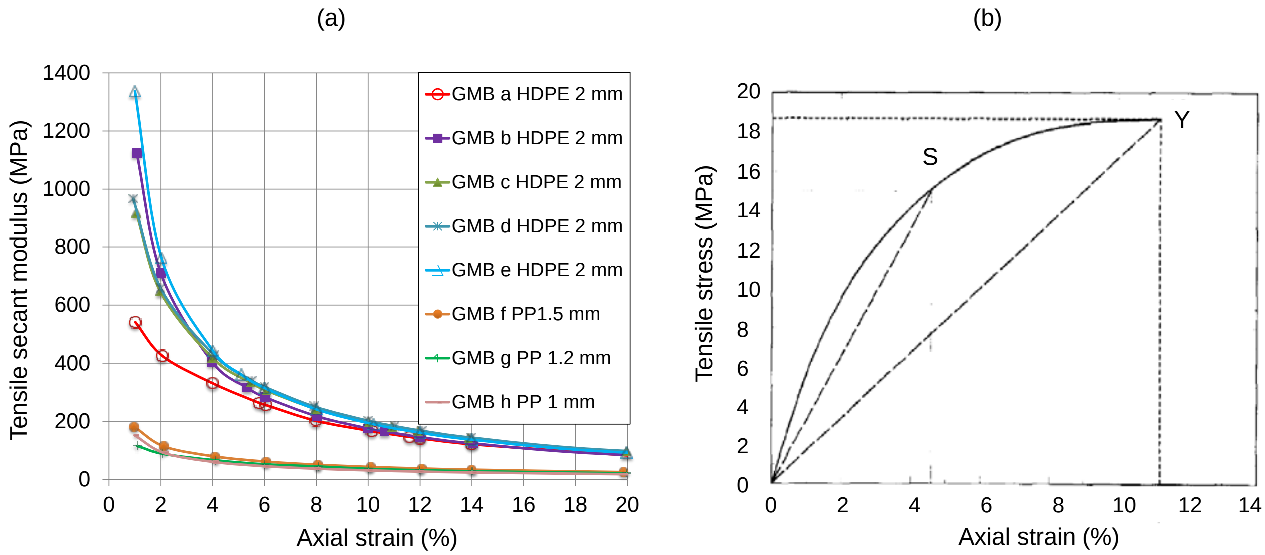

Figure 7. (a) Tensile secant modulus as a function of the axial strain for several GMBs. (b) Initial portion of typical stress-strain curve for HDPE GMB from the origin to the yield peak (Y). The letter “S” indicates the secant line (Giroud, 1994).

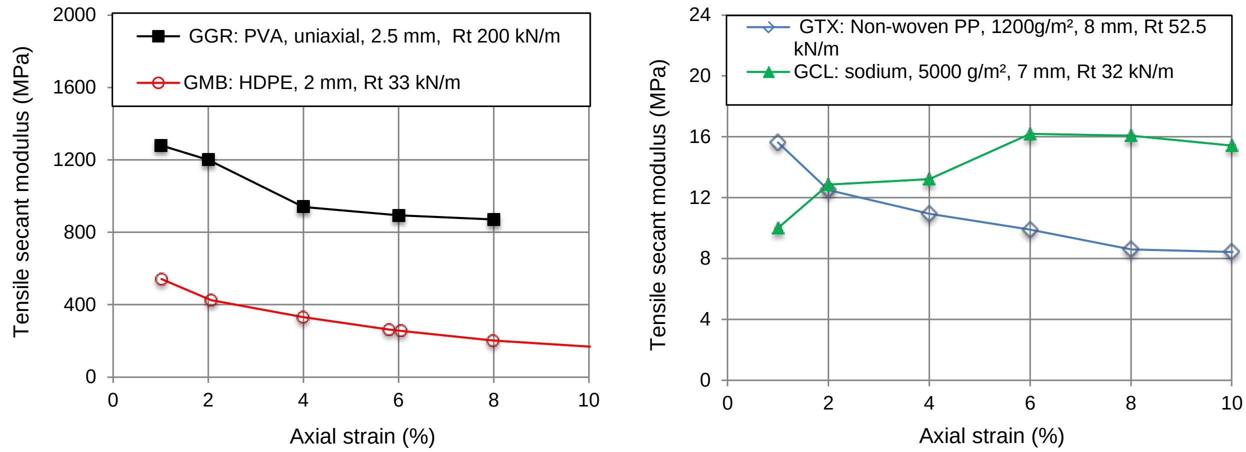

Figure 8. Tensile secant modulus as a function of axial strain for geosynthetics used in this study.

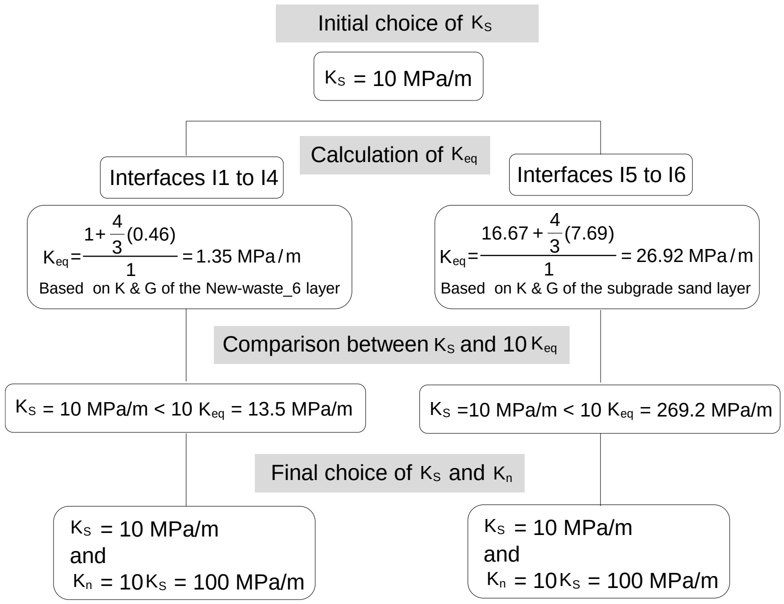

Figure 9. Procedure recommended by Itasca for the choosing between shear and normal interface stiffness.

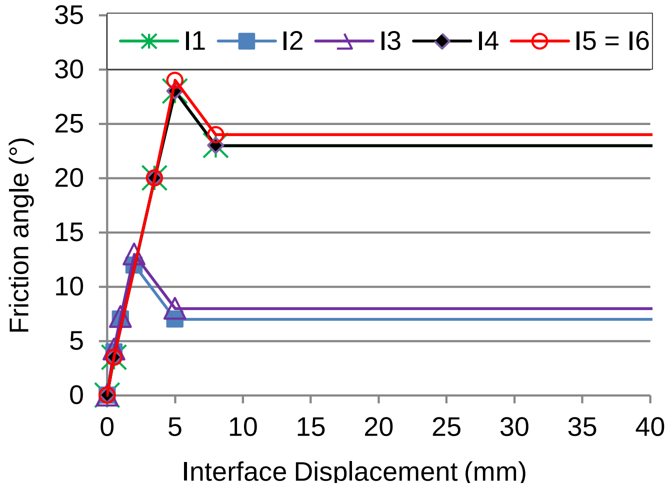

Figure 10. Friction angle as a function of interface displacement for the six interfaces used in this study.

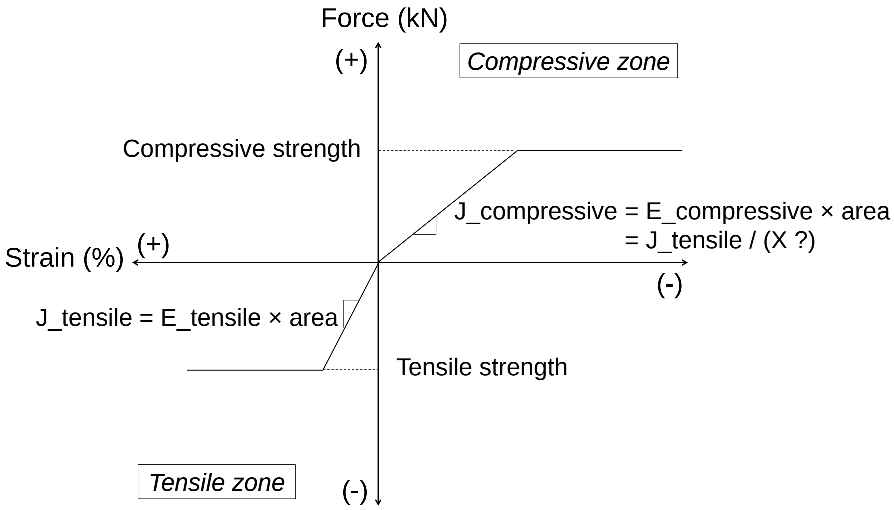

Figure 11. Diagram showing characteristics of GSY in force-strain parameter space.

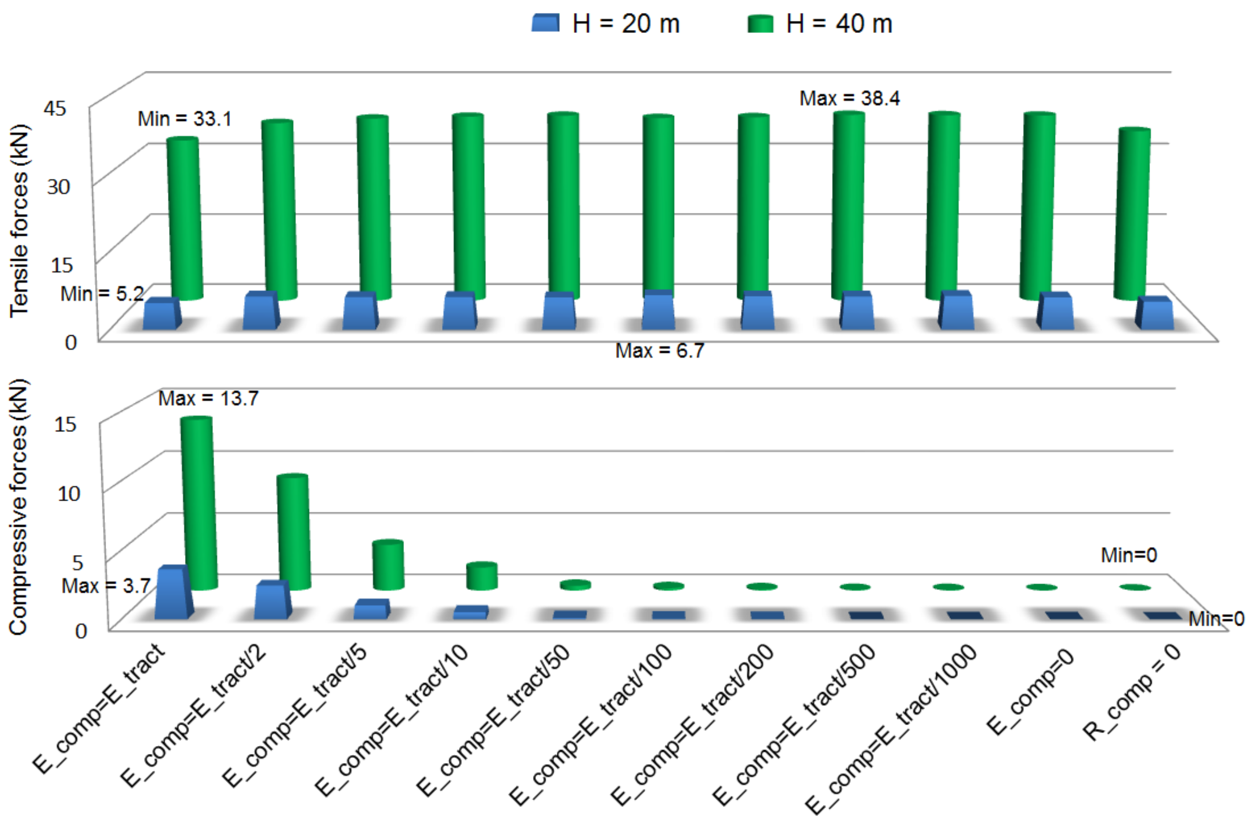

Figure 12. Simulation results for tensile and compressive forces in GMB for the 11 cases investigated in this study.

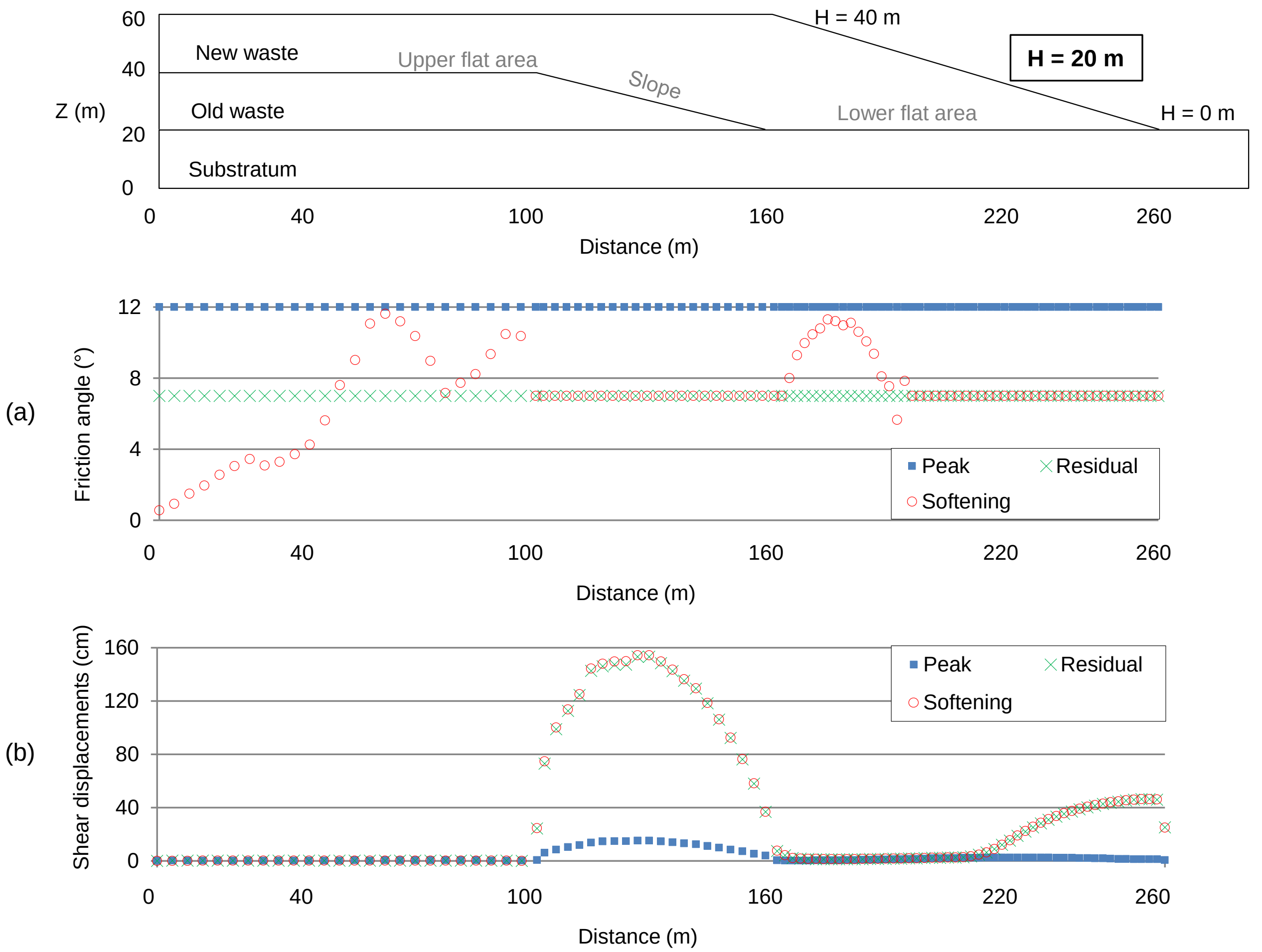

Figure 13. (a) Friction angle as a function of distance along interface I2 for H = 20 m. (b) Shear displacement as a function of distance along interface I2 for H = 20 m.

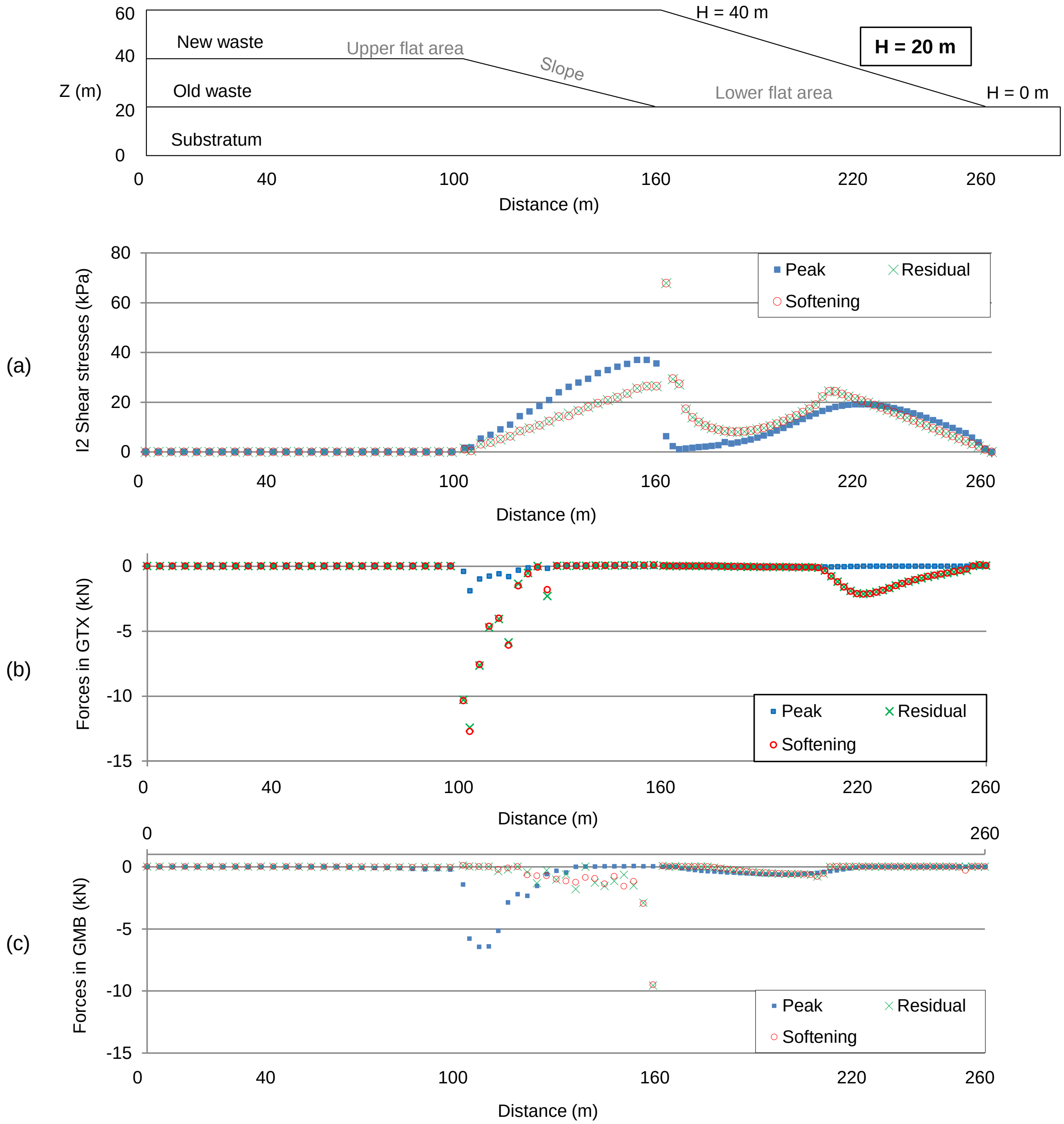

Figure 14. (a) Shear stress as a function of distance along interface I2 (GTX-GMB) for H = 20 m. (b) Axial force as a function of distance in the geotextile (GTX) for H = 20 m. (c) Axial force as a function of distance in geomembrane (GMB) for H = 20 m.

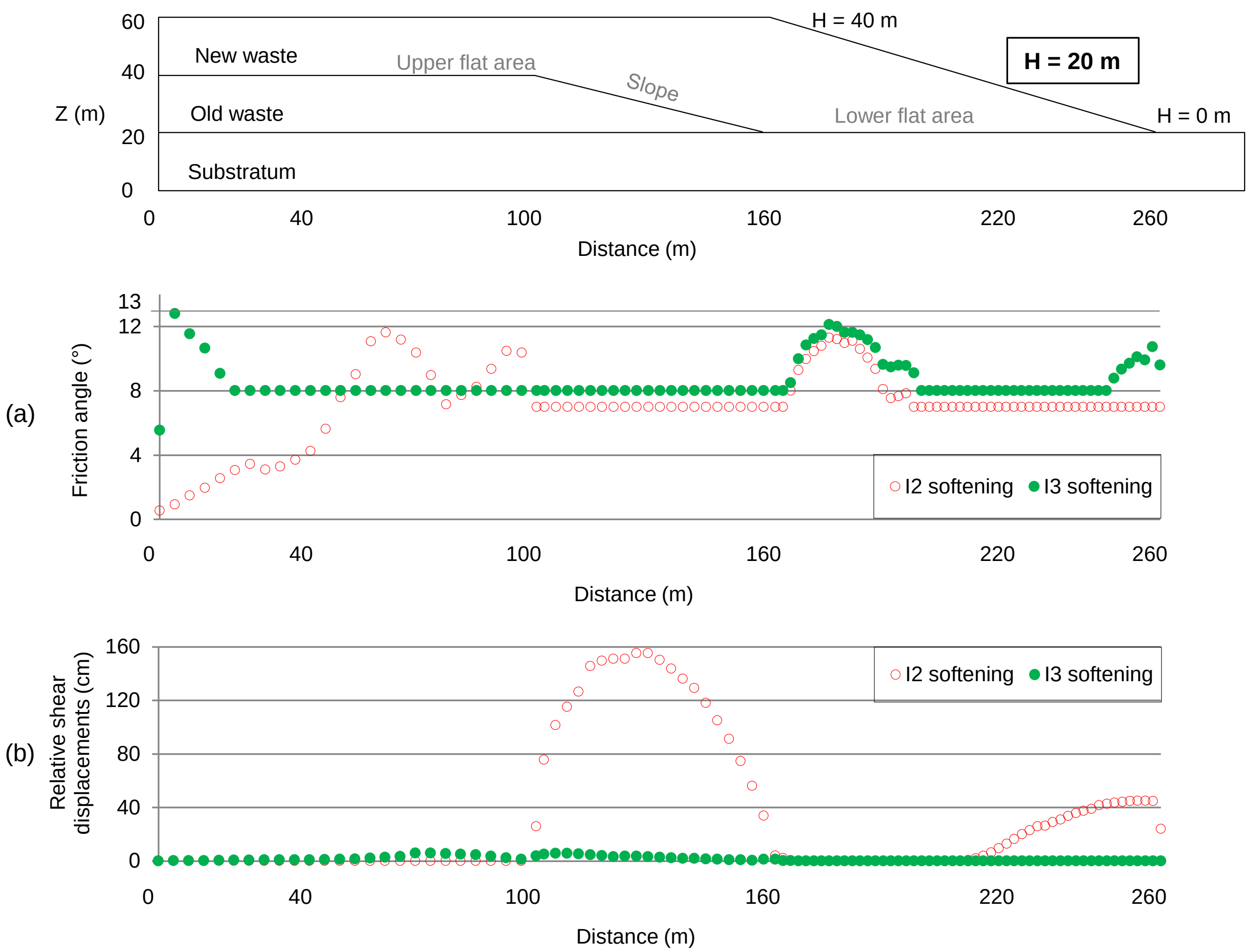

Figure 15. Comparison of I2 and I3: (a) Friction angle as a function of distance along interface I2 (GTX-GMB) and interface I3 (GMB-GCL) for H = 20 m. (b) Relative shear displacements as a function of distance along interface I2 (GTX-GMB) and interface I3 (GMB-GCL) for H = 20 m.

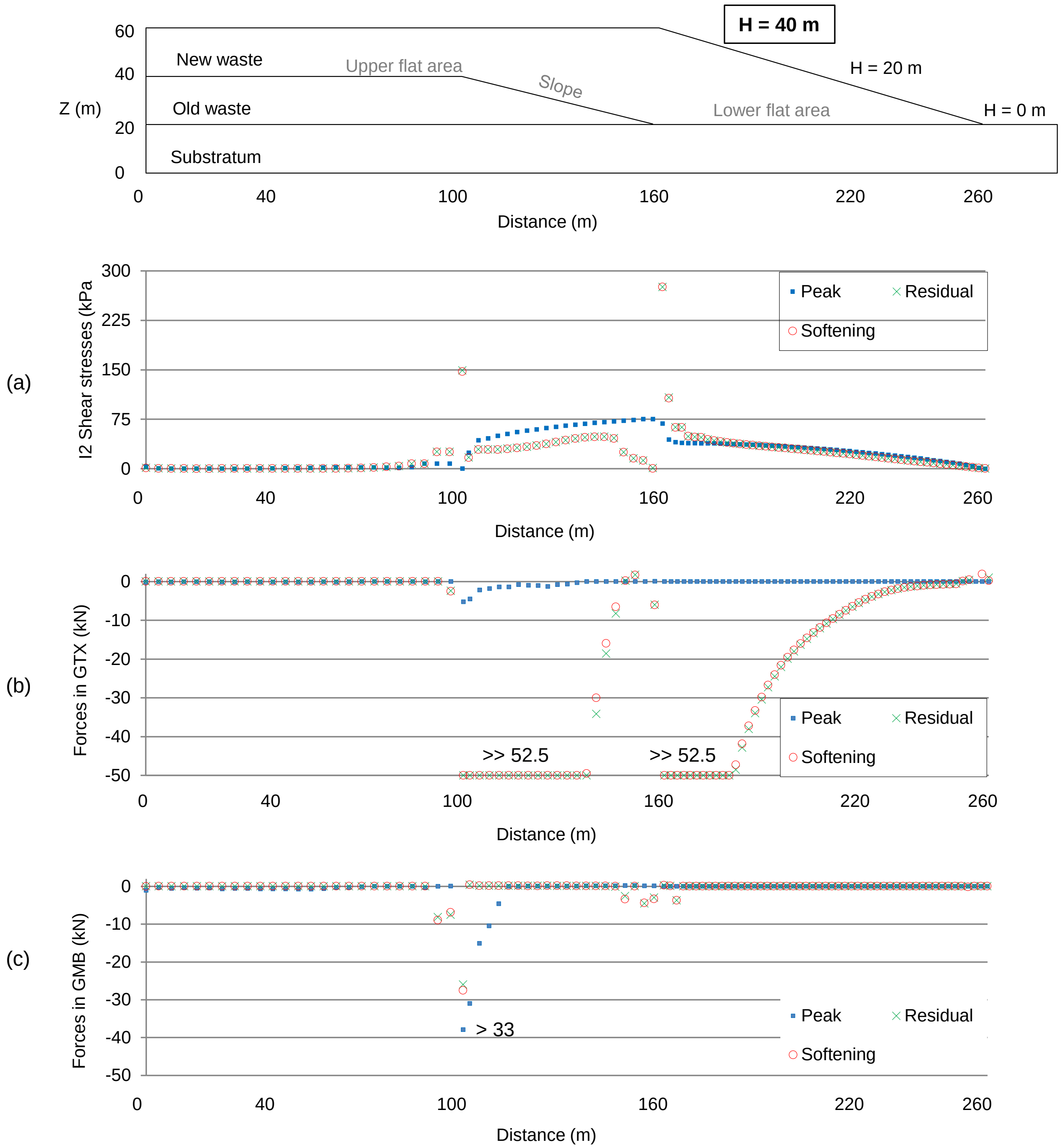

Figure 16. (a) Shear stress as a function of distance along interface I2 (GTX-GMB) for H = 40 m. (b) Axial force as a function of distance in the geotextile (GTX) for H = 40 m. (c) Axial force as a function of distance in geomembrane (GMB) for H = 40 m.

Table 1. Summary of numerical studies involving interactions between geosynthetics.

References	CR1	CR2	CR3	CR4	CR5
Wilson-Fahmy and Koerner (1993)	2 / 3	✓	✓		
Byrne (1994)	0 / 1	✓	✓		
Long et al. (1995)	3 / 5		✓	✓	✓
Richardson and Marr (1996)	1 / 2	✓			
Reddy et al. (1996)	0 / 1	✓	✓		
Villard et al. (1999)	2 / 3	✓		✓	
Jones et al. (2000)	0 / 1	✓	✓		
Meissner and Abel (2000)	2 / 2	✓	✓		
Connell (2002)	0 / 1		✓		
Filz et al. (2001)	0 / 2	✓	✓		
Jones and Dixon (2005)	0 / 1	✓	✓		
Fowmes et al. (2005a)	2 / 3		✓	✓	
Fowmes et al. (2005b)	2 / 3	✓	✓	✓	
He et al. (2006)	2 / 3	✓		✓	
Chugh et al. (2007)	0 / 1	✓	✓		
Haque (2007)	0 / 0	✓			
Fowmes et al. (2008)	2 / 3	✓	✓	✓	
Wu et al. (2008)	1 / 1				
Chen et al. (2009a)	3 / 6				

Gao (2009), Chen et al. (2009b) et Chen et al. (2011)	1 / 2				
Arab et al. (2011a)	1 / 2	✓			
Rong et al. (2011)	?	✓			
Sia and Dixon (2012)	2 / 3	✓	✓		
Zamara et al. (2014)	2 / 3	✓	✓	✓	
Present study	4 / 6	✓	✓	✓	✓

CR1: Number of GSY and interfaces in the model.

CR2: Staged construction or evolution of the waste properties with depth or stress.

CR3: Strain softening at interfaces.

CR4: Differentiation between the compressive and tensile characteristics of GSY.

CR5: Evolution with strain of GSY axial stiffness.

Table 2. Various published values of unit weight of waste.

γ (kN/m³)	Comments	References
6	MSW with 2-m-thick layer compacted by 21 t roller	Watts and Charles (1990)
8	MSW with 0.6-m-thick layer compacted by 21 t roller	
10	At 3 m depth	Oweiss and Khera (1990)
15	At 55 m depth	
3–9	Low compaction	Fasset et al. (1994)
5-7.8	Medium compaction	
8.8-10.5	Good compaction	
10.2	Cincinnati Site	Eid et al. (2000)
6-7	Fresh waste just after compaction	Kavazanjian (2001)
14-20	Degraded waste with high soil content	
12.23		Jones and Dixon (2005)
8.8	On Cruz das Almas Maceio site in Brazil	Gharabaghi et al. (2008)
14.7	On Cruz das Muribeca Recife site in Brazil	
9.4	From a site in France at 4-6 m depth	Stoltz et al. (2009)
16	from a site in France at 27-32 m depth	

7.8	from a site in France, aged 8 years under 200 kPa	Ecogeos (2011)

Table 3. Various published values of elastic parameters of waste.

E (MPa)	ν	Comments	References
NA	0.49	From compressional and shear wave velocities in liquid and solid waste in San Pablo Bay, Richmond, California, USA	Sharma et al. (1990)
NA	0.33	From compressional and shear wave velocities - Mean value retained because of significant scatter	Matasovic and Kavazanjian (1998)
NA	0.36	Specific for drained waste with high permeability	Abbiss (2001)
0.5	0.3	NA	Jones and Dixon (2005)
NA	0.29-0.46	From compressional and shear wave velocities in a bioreactor	Carpenter et al. (2013)
0.5-0.7	0.05-0.15	Degradable and compressible (food, green waste, etc.)	Singh and Fleming (2008)
1.5-3	0.28-0.32	Paper, cards, plastics	
10-20	0.25-0.33	Rubble, cover soil, and ashes	
0.7	0.45	Coll Cardús landfill, Spain: during construction	Yu and Batlle (2011)
7	0.3	Coll Cardús landfill, Spain: After construction	

E (MPa)	ν	Comments	References
0.5	NA	Coll Cardús landfill, Spain: long term	Varga (2011a)
NA	0.25	1st phase of degradation : lag phase	
NA	0.45	5th phase of degradation : Maturation phase	
0.5	0.3	Milegate landfill, United Kingdom	Zamara et al. (2014)

NA: Not available.

Table 4. Various published values of the cohesion and friction angle of waste.

c (kPa)	Φ (°)	Comments	References
0	24-42	Small triaxial test (TT)	Stoll (1971)
10 - 23	24-42	Direct shear test (DST) on several samples from landfills in Canada	Landva and Clark (1986)
0	39-53	DST at 10% of tangential displacement	Siegel et al. (1990)
10	25	Retrospective analysis (RA), trench in waste mass	Cowland et al. (1993)
2-3	15-20	Large TT at 10%-15% of axial strain	Grisolia et al. (1995a)
24	0	RA, normal stress <30 kPa	Kavazanjian et al. (1995)
0	30	RA, normal stress >30 kPa	
0-28	20-39	Not available	Gabr and Valero (1995)
25	35	Large DST + RA of four slope failures	Eid et al. (2000)
27	42	DST	Edincliler et al. (1996)
39.2	29	At natural moisture content and 20% strain	Vilar and Carvalho (2002)
60.7	23	Saturated sample at 20% strain	
67	23	Large DST	Caicedo et al. (2002)
2.5-4	21-36	DST	Mahler and De Lamare Netto (2003)

c (kPa)	Φ (°)	Comments	References
9-14	20-29	DST and large TT	Harris et al. (2006)
0	36-41	TT at confining pressure of 200 kPa	Zekkos et al. (2006)
0	35-37	Large TT	Zwanenburg et al. (2007)
0-8.4	35-47	Large TT	Singh et al. (2009)
0-85.9	2.4-34.1	DST at 10% strain on a waste aged 5 to 8 years from a site in France	Ecogeos (2011)

Table 5. Summary of the material properties used in this study.

<table>
<tr><th colspan="6">MATERIALS PROPERTIES</th></tr>
<tr><th>Type</th><th>γ (kN/m³)</th><th>E (MPa)</th><th>ν</th><th>c (kPa)</th><th>Φ (°)</th></tr>
<tr><td>New waste</td><td>9.0 to 12.6</td><td>0.5 to 1.0</td><td>0.2 to 0.3</td><td>10.0 to 5.0</td><td>30.0 to 25.0</td></tr>
<tr><td>Old waste</td><td>10.0 to 12.8</td><td>1.0 to 1.2</td><td>0.3 to 0.4</td><td>5.0 to 3.0</td><td>24.0 to 22.0</td></tr>
<tr><td>Subgrade layer</td><td rowspan="2">18</td><td>20</td><td rowspan="2">0.3</td><td>0</td><td>35</td></tr>
<tr><td>Clay substratum</td><td>50</td><td>5</td><td>28</td></tr>
</table>

Table 6. Summary of properties used in this study for geosynthetics.

GEOSYNTHETIC PROPERTIES			
Type	e (mm)	E at 1% strain (MPa)	E at 10% strain (MPa)
GTX	8	15.6	8.4
GMB	2	541.2	166.0
GCL	7	10.0	15.4
GGR	2.5	1280.0	870.0

Table 7. Various published values of cohesion and friction angle of interfaces involving geosynthetics.

Interface type	c_{peak} (kPa)	Φ_{peak} (°)	c_{res} (kPa)	Φ_{res} (°)	Comments	References
GTX-GMB dry	NA	12.5	NA	9	NA	Seed et al. (1988)
GTX-GMB wet	NA	10.4	NA	8	NA	
GTX-GMB	NA	14	NA	12	NA	Byrne et al. (1992)
GTX-GMB	0	8.5	0	6	Torsional ring shear test (TRST)	Stark and Poeppel (1994)
GTX-GMB	1.4	11	NA		Direct shear test (DST) : 0.3 m × 0.3 m	Reddy et al. (1996)
GTX-GMB	NA		0	12	DS : 0.3 m × 0.3 m and large displacement (LD) = 2 mm	Villard et al. (1999)
GTX-GMB dry HDPE	0	7.76	0	7.41	DST: 0.3 m × 0.3 m LD = 50 mm	Bergado et al. (2006)
GTX-GMB wet HDPE	0	9.46	0	8.96		
GTX-GMB	8.2	27.5	5.6	16.5	DST: 0.3 m × 0.3 m and	Fowmes et al.
LLDPE	1	29	2	18.8	under σ = 10, 30 and 50	(2008)

GTX-GMB HDPE	0.4	11.7	0.4	9	kPa and LD = 80 mm	
GTX-GMB	NA		5	12.8	DST: 0.3 m × 0.3 m and under σ = 50, 100 et 200 kPa and LD = 90 – 100 mm	Chen et al. (2010), Chen et al. (2011)
GTX-GMB textured dry	2.3	19.9	1.4	13.3	DST under σ = 10, 25, 50, 100 and 200 kPa	Zamara et al. (2014)
GTX-GMB textured wet	4	20.8	2.9	14.7		
GTX-GMB textured	12	30	NA		DST: 0.3 m × 0.3 m	Reddy et al. (1996)
GTX-GMB textured HDPE	NA	32	NA	13	TRS under σ = 50 to 280 kPa	Stark et al. (1996)
GTX-GMB textured	3.2	24.5	2.5	12.8	DST: 0.3 m × 0.3 m under σ = 25, 50, 100 and 200 kPa and LD = 9.3 to100 mm	Jones and Dixon (2005)
GTX-GMB textured	8	29.4	5.4	18.7	DST: 0.3 m × 0.3 m under σ = 10, 30 and 50 kPa and LD = 80 mm	Fowmes et al. (2008)

GTX-GMB textured HDPE	NA	18.9-34.8	NA	15-18.4	TRST under σ = 50 to 300 kPa	Effendi (2011)
GMB-GCL wet	0	6.49	0	6.49	DST: 0.3 m × 0.3 m LD = 50 mm	Bergado et al. (2006)
GMB-GCL dry	0	8.93	0	8.93		
GMB-GCL	NA		11.4	23.6	DST: 0.3 m × 0.3 m under σ = 50, 100 and 200 kPa and LD = 90 – 100 mm	Chen et al. (2011)
GMB-GCL wet	0	20.9	5	9.3		
GMB-GCL dry	0	24.4	0	16.9		
GMB-Clay	NA		0	9	DST : 0.3 m × 0.3 m and LD = 2 mm	Villard et al. (1999)
GMB-Clay undrained	31.1	7.6	3.2	25.1	DST under σ = 10, 25, 50, 100 and 200 kPa	Zamara et al. (2014)
GMB-Clay drained	8	22	8	22		
Granular soil-GTX	NA		0	29	DST: 0.3 m × 0.3 m and LD = 2 mm	Villard et al. (1999)
GTX-waste	4.4	29.9	3.3	29.8	DST : 0.3 m × 0.3 m under σ = 10, 30 and 50 kPa and LD = 80 mm	Fowmes et al. (2008)
Sand-GTX dry	6.3	29.9	1.8	29.6	DST under σ = 10, 25, 50, 100 and 200 kPa	Zamara et al. (2014)
Sand-GTX wet	3.2	29.9	1.3	29.6		
Waste-Sand	5	20	5	20		

GGR-Aggregates	0	48	NA		DST under σ = 3470, 5860 and 10580 lb	Bakeer et al. (1998)
GGR–Crushed rock		31-54	NA		DST: 0.3 m × 0.3 m under σ = 50. 100 and 150 kPa	Baykal and Dadasbilge (2008)
GGR-Sand		34.9-36	NA		Large plane strain compression 0.56 m × 0.56 m × 0.45 m	Liu et al. (2014)
GGR-Expanded clay	4.3	39	0.7	32	DST: 0.3 m × 0.3 m under σ = 13.8, 27.6, and 41.34 kPa	Yuan (2002)

NA: Not available.

Table 8. Summary of properties used in this study for interfaces

INTERFACE PROPERTIES					
Type	K_s (MPa/m)	K_n (MPa/m)	c (kPa)	Φ_{peak} (°)	Φ_{res} (°)
I1: New Waste-GTX*				28[a]	23
I2: GTX-GMB				12[b]	7
I3: GMB-GCL	10	100	0	13[b]	8
I4: GCL-Subgrade layer				28[a]	23
I5 and I6: GGR-Subgrade layer				29[a]	24

* The values mentioned correspond to the contact between a drainage gravel layer under new waste and the GTX.

[a]: reached at 5 mm of relative shear displacement

[b]: reached at 2 mm of relative shear displacement

8. REFERENCES

Abbiss, C.P., 2001. Deformation of landfill from measurement of shear wave velocity and damping Geotechnique. 51(6), 483 - 492.

Afnor,2008. NF EN ISO 10319 : Géosynthétiques - Essai de traction des bandes larges. 11 p.

Afnor,2013. NF EN 12311-2 : Feuilles souples d'étanchéité - Détermination des propriétés en traction - Partie 2 : Feuilles d'étanchéité de toiture plastiques et élastomères. 9 p.

Arab, M.G., Kavazanjian, E., Matasovic, M., 2011a. Seismic analysis of geosynthetic liner system. Proc. of the Geo-frontiers ASCE 2011, Dallas, Texas, USA, pp. 1981-1990.

Bakeer, R.M., Sayed, S.M., Cates, P., Subramanian, R., 1998. Pullout and shear tests on geogrid reinforced lightweight aggregate. Geotextiles and Geomembranes. 16, 119-133.

Baykal, G., Dadasbilge, O., 2008. Experimental investigation of pull-out resistance of uniaxial geogrids. Proc. of the 4th Asian Regional Conference on Geosynthetics, Shanghai, China, pp. 174-178.

Beaven, R.P., Powrie, W., 1995. Hydrogeological and geotechnical properties of refuse using a large scale compression cell. Proc. of the Sardinia 1995, Fifth International Waste Management and Landfill Symposium, pp. 745-760.

Bergado, D.T., Ramana, G.V., Sia, H.I., Varun, 2006. Evaluation of interface shear strength of composite liner system and stability analysis for a landfill lining system in Thailand. Geotextiles and Geomembranes. 24(6), 371-393.

Bray, J.D., Zekkos, D., Kavazanjian Jr., E., Athanasopoulos, G.A., Riemer, M.F., 2009. Shear Strength of Municipal Solid Waste. Journal of Geotechnical and Geoenvironmental Engineering, 14 p.

Byrne, J.R., Kendall, J., Brown, S., 1992. Cause and mechanism of failure of Kettleman Hills landfill B-19, Phase IA. Stability and Perf. of Slopes and Embankments, ASCE. 2, 1188-1215.

Byrne, R.J., 1994. Design issues with strain-softening interfaces in landfill liners. Proc. of the Waste Technology 94, Charleston, South Carolina, USA, Session 4,Paper 4. 26 p.

Carpenter, P.J., Reddy, K.R., Thompson, M.D., 2013. Seismic Imaging of a Leachate-Recirculation Landfill: Spatial Changes in Dynamic Properties of Municipal Solid Waste. Journal of Hazardous, toxic and radioactive waste, ASCE, 331-341.

Carucci, A., Gabrielli, B., Grisolia, M., 1991. Stability of slopes in a sanitary landfill. Proc. of the Sardinia 91,2 - 3rd International Landfill Symposium, Cagliari (I):CISA, pp. 1161-1170.

Castelli, F., Maugeri, M., 2008. Experimental analysis of waste compressibility. Geotechnical Special Publication, ASCE. 177, 208-215.

Chen, Y.-M., Tang, X., Zhang, L., 2009a. Old landfill expansion in the vertical expansion. Proc. of the International Symposium on Geoenvironmental Engineering, Hangzhou, China, pp. 80-89.

Chen, Y.-M., Gao, D., Zhu, B., 2009b. Controlling strain in geosynthetic liner systems used in vertically expanded landfills. Journal of Rock Mechanics and Geotechnical Engineering 2009. 1(1), 48-55.

Chen, Y.-M., Lin, W.-A., Zhan, T.L.T., 2010. Investigation of mechanisms of bentonite extrusion from GCL and related effects on the shear strength of GCL/GM interfaces. Geotextiles and Geomembranes. 28(1), 63-71.

Chen, Y.M., Lin, W.A., Zhu, B., Zhan, L.T., 2011. Performance-based Design for Geosynthetic Liner Systems in Landfills. Geotechnical Engineering Journal of the SEAGS & AGSSEA 2011. 42(1), 7p.

Chugh, A.K., Stark, T.D., De-Jong, K.A., 2007. Reanalysis of a municipal landfill slope failure near Cincinnati, Ohio, USA Canadian Geotechnical Journal. 44, 33-53.

Connell, A.C.,2002. Factors controlling the waste/barrier interaction with specific consideration to the integrity of steep-sided landfill lining systems. Department of Civil and Building Engineering, Loughborough University. Loughborough University internal report submitted in partial fulfilment of transfer from MPhil to PhD.

Cowland, J.W., Tang, K.Y., Gabay, J., 1993. Density and strength properties of Hong Kong refuse. Proc. of the 4th International Waste Management and Landfill Symposium, Cagliari, Italy, pp. 1433-1446.

Criley, K.R., Saint John, D., 1997. Variability analysis of soil vs. geosynthetic interface friction characteristics by multiple direct shear testing. Proc. of the Geosynthetics 1997, Long Beach, CA, pp. 885-897.

Del Greco, O., Oggeri, C., 1993. Geotechnical parameters of sanitary wastes. Proc. of the Sardinia 1993, Fourth International Landfill Symposium, Cagliari, Italy, pp. 1421-1431.

Dixon, N., Jones, R.R.V., Fowmes, G.J., 2006. Interface shear strength variability and its use in reliability-based landfill stability analysis. Geosynthetics international. 13(1), 1-14.

Ecogeos, 2011. Etude géotechnique dans le cadre d’un projet d’extension d’ISDND en Ile de France, Résultats des investigations de terrain et des essais de laboratoire, unpublished. 44 p.

Effendi, R., 2011. Geomembrane-Geotextile Interface Friction. Jurnal Teknologi Berkelanjutan. 1(1), 1-8.

Eid, H.T., Stark, T.D., Evans, W.D., Sherry, P.E., 2000. Municipal solid waste slope failure - I: Waste and foundation soil properties. Journal of Geotechical and Geoenvironmental Engineering, ASCE. 156(5), 397-407.

Eid, H.T., 2011. Shear strength of geosynthetic composite systems for design of landfill liner and cover slopes. Geotextiles and Geomembranes. 29(3), 335-344.

Fasset, J.B., G.A., L., P.C., R., 1994. Geotechnical properties of municipal solid waste and their use in landfill design. Proc. of the Waste technical conference, Charleston, pp. 1-31.

Filz, G.M., Esterhuizen, J.J.B., Duncan, J.M., 2001. Progressive failure ol lined waste impoundments. Journal of Geotechnical and Geoenvironmental Engineering, ASCE. 127, 841-848.

Fleming, I.R., Sharma, J.S., Jogi, M.B., 2006. Shear strength of geomembrane-soil interface under unsaturated conditions. Geotextiles and Geomembranes. 24, 274-284.

Fowmes, G.J., Zhang, B., N. Dixon, El-Hamalawi, A., Jones, D.R.V., 2005a. Modelling of Waste Barrier Interaction. Proc. of the International Workshop, LIRIGM, Grenoble 1 University, France. 4 p.

Fowmes, G.J., Jones, D.R.V., Dixon, N., 2005b. Analysis of a landfill directive compliant steepwall lining system. Proc. of the 10th International Waste Management and Landfill Symposium, Sardinia, S. Margherita di Pula, Cagliari, Italy, pp. 369.

Fowmes, G.J.,2007. Analysis of steep sided landfill lining systems. Univ. of Loughborough, England. Dissertation in partial fulfilment of the requirements for the award Engineering Doctorate, PhD thesis, 261 p.

Fowmes, G.J., Dixon, N., Jones, D.R.V., 2008. Validation of a numerical modelling technique for multilayered geosynthetic landfill lining systems. Geotextiles and Geomembranes 26, 109-121.

Gabr, M.A., Valero, S.N., 1995. Geotechnical properties of solid waste. Geotechnical Testing Journal, ASTM. 18(2), 241-251.

Gao, D.,2009. Deformation and Stability of Intermediate Liner for Landfill Expansion and Controlling Measures. Univ. of Zhejiang, Hangzhou. PhD thesis, 267 p.

Girard, H., Fisher, S., Alonso, E., 1990. Problem of friction posed by the use of geomembranes on dam slopes-examples and measurements. . Geotextiles and Geomembranes. 9, 129-143.

Giroud, J.P., 1994. Mathematical model of geomembrane stress-strain curves with a yield peak. Geotextiles and Geomembranes. 13(1), 1-22.

Giroud, J.P., Beech, J.F., , 1989. Stability of soil layers on geosynthetic lining system. Proc. of the Geosynthetics Conference, San Diego, USA, pp. 35-46.

Gourc, J.P., Olivier, F., Thomas, S., Chatelet, L., Denecheau, P., Lmunoz, M., 2001. Monitoring of waste settlements on five landfills: comparison of the efficiency of different devices Proc. of the Sardinia ’01, Eighth International Waste Management and Landfill Symposium, Cagliari, Italy, pp. 515-524.

Grisolia, M., Napoleoni, Q., Tancredi, G., 1995a. The use of triaxial test for the mechanical characterization of MSW. Proc. of the Sardinia 95, Fifth International Waste Management and Landfill Symposium, pp. 761-768.

Haque, M.A.,2007. Dynamic characteristics and stability analysis of municipal solid waste in bioreactor landfills. Univ. of Texas at Arlington. Partial Fulfillment of the Requirements for the Degree of Doctor of philosophy, PhD thesis, 167 p.

He, P., Girard, H., Poulain, D., Lac, P., 2006. Modélisation numérique du comportement mécanique sur pente des dispositifs d'étanchéité par géomembranes. Proc. of the Rencontres Géosynthétiques 2006, Montpellier, France, pp. 191-198.

Itasca,2005. FLAC Version 5, Fast Lagrangian Analysis of Continua, Online Manual Table of Contents. 3058.

Izgin, M., Wasti, Y., 1998. Geomembrane-sand interface frictional properties as determined by inclined board and shear box tests. Geotextiles and Geomembranes. 16, 207-219.

Jessberger, H.L., Kockel, R., 1993. Determination and assessment of the mechanical properties of waste materials. Proc. of the Sardinia 1993, Fourth International Landfill Symposium, Cagliari, Italy, pp. 167-177.

Jones, D.R.V., Dixon, N., Connell, A., 2000. Effect of Landfill Construction Activities on Mobilised Interface Shear Strength. Proc. of the Second European Geosynthetics Conference, Eurogeo, Bologna, Italy.2. 14 p.

Jones, D.R.V., Dixon, N., 2005. landfill lining stability and integrity: the role of waste settlement. Geotextile and Geomembranes. 23, 27-53.

Kavazanjian, E., 2001. Mechanical properties of municipal solid waste. Proc. of the Sardinia 01, Eighth International Waste Management and Landfill Symposium, Cagliari, Italy, pp. 415-424.

Kavazanjian, J.E., Matasovic, N., Bonaparte, R., Schmertmann, G.R., 1995. Evaluation of MSW Properties for Seismic Analysis. Geoenvironment 2000, Geotechnical Special Publication ASCE. 46, 1126-1141.

Koerner, R.M., Hwu, B.-L., 1991. Stability and tension considerations regarding cover soils on geomembrane lined slopes. Geotextiles and Geomembranes. 10(4), 335-355.

Koerner, R.M., Koerner, G.R., 2001. Geosynthetics design beyond factor of safety; risk assessment using probability of failure analysis. Proc. of the GRI-15, Hot Topics in Geosynthetics-II, Houston, USA, pp. 235-253.

Kölsch, F., 1993. The bearing behaviour of domestic waste and related consequence for stability. Proc. of the Sardinia 93, 4th International Landfill Symposium, Cagliari, Vol. II, pp. 1393-1410.

Landva, A., Clark, J.I., 1986. Geotechnical testing of waste fill. Proc. of the Canadian geotechnical Conference, Ottawa, Ontario, pp. 371-385.

Le Hello, B.,2007. Renforcement par géosynthétiques des remblais sur inclusions rigides, étude expérimentale en vrai grandeur et analyse numérique. Univ. de Grenoble. PhD thesis, 234 p.

Linsley, R.K., Kohler, M.A., Paulhus, J.L.H., 1982. Hydrology for Engineers, McGraw-Hill Book Co. New York. 3rd édition. 512 p.

Liu, C.-N., Yang, K.-H., Nguyen, M.D., 2014. Behavior of geogrid reinforced sand and effect of reinforcement anchorage in large-scale plane strain compression. Geotextiles and Geomembranes. 42, 479-493.

Long, J.H., Gilbert, R.B., Daly, J.J., 1995. Effect of waste settlement on slope lining system. Proc. of the Geosynthetics 95, Nashville, Tennessee, USA.3, pp. 729-744.

Mahler, C.F., De Lamare Netto, A., 2003. Shear resistance of mechanical biological pre-treated domestic urban waste. Proc. of the Sardinia 03, 9th International Waste Management and Landfill Symposium, Cagliari, Italy. 8 p.

Matasovic, N., Kavazanjian, E.J., 1998. Cyclic characterization of OII landfill solid waste. Journal of Geotech. Geoenviron. Eng. 124(3), 197-210.

Mccartney, J.S., Zornberg, J.G., Swan, R.H.J., Gilbert, R.B., 2004. Reliability-based stability analysis considering GCL shear strength variability. Geosynthetics international. 11(3), 212-232.

Meissner, H., Abel, K.,2000. Numerical investigations of inclined landfill liner systems. GeoEng2000, Melbourne, Australia. published on CD.

Murthy, V.N.S., 2002. Geotechnical Engineering: Principles and Practices of Soil Mechanics and foundation engineering, CRC Press. 1rd édition. 1056 p.

Myles, B., 1982. Assessment of soil fabric friction by means of shear Proc. of the Second International Conference on Geotextiles, Las Vegas.3, pp. 787-791.

Oweiss, I.S., Khera, R.P.,1990. Geotechnology of Waste Management, Butterworth & Co. (Publishers) Ltd., Kent, England. 273.

Palmeira, E.M., 2009. Soil–geosynthetic interaction: Modelling and analysis. Geotextiles and Geomembranes. 27, 368-390.

Reddy, K.R., Kosgi, S., E.S.Motan, 1996. Interface shear behavior of landfill composite liner systems: A finite element analysis. Geosynthetics international. 3(2), 247-275.

Richardson, G.N., Marr, W.A., 1996. Geotechnical Considerations for the Design of Piggy Backed Lined Landfills. Proc. of the 3rd International Symposium on Environmental Geotechnology, San Diego, USA, pp. 550-558.

Rong, F., Zhaogui, G., Tugen, F., 2011. Analysis of Stability and Control in Landfill Sites Expansion. Proc. of the Procedia Engineering 24, International Conference on Advances in Engineering, pp. 667-671.

Seed, R.B., Mitchell, J.K., Seed, H.B.,1988. Slope stability failure investigation: landfill unit B-19, phase I-A, Kettleman Hills, California Rep. No. UCB/GT/88-01, University of California, Berkeley,Calif.

Sharma, H.D., Dukes, M.T., Olsen, D.M., 1990. Field Measurements of Dynamic Moduli and Poisson's Ratio of Refuse and Underlying Soils at a Landfill Site. Geotechnics of Waste Fills – Theory and Practice, STP 1070, ASTM, Philadelphia, PA.

Sia, A., Dixon, N., 2012. Numerical modelling of landfill lining system waste interaction: implications of parameter variability. Geosynthetics international. 19(5), 393-408.

Siegel, R.A., Robertson, R.J., Anderson, D.G., 1990. Slope stability investigations at a landfill in Southern California. Geotechnics of Waste Fill - Theory and Practice, American Society for Testing and Materials (ASTM) STP 1070, 259-284.

Singh, M.K., Fleming, I.R., 2008. Estimation of the mechanical properties of MSW during degradation in a laboratory compression cell. Geotechnical Special Publication, ASCE. 177, 200-207.

Singh, M.K., Sharma, J.S., Fleming, I.R., 2009. A design chart for estimation of horizontal displacement in municipal landfill. Waste Management. 29, 1577-1587.

Singh, S., Murphy, B.J., 1990. Evaluation of the Stability of Sanitary Landfills. Geotechnics of Waste Fills - Theory and Practice, ASTM STP 1070, 240-258.

Sitharam, T.G., Srilakshmi, G., Sireesh, S., 2006. Numerical Simulation of Geocell Reinforced Sand Beds using FLAC3D – 2006 – Proc. of the 4th International FLAC Symposium on Numerical Modeling in Geomechanics .Hart & Varona (eds.) Paper: 05-04, © 2006 Itasca Consulting Group, Inc., Minneapolis, ISBN 0-9767577-0-2. 8 p.

Stark, T.D., Poeppel, A.R., 1994. Landfill Liner Interface Strengths from Torsional-Ring-Shear Tests”. Journal of geotechnical engineering, American Society of Civil Engineers. 120(3), 597-615.

Stark, T.D., Williamson, T.A., Eid, H.T., 1996. Geomembrane/geotextile interface shear strength. Journal of geotechnical engineering, American Society of Civil Engineers. 122(3), 197-203.

Stoewahse, C., Dixon, N., Jones, D.R.V., Blümel, W., Kamugisha, P., 2002. Geosynthetic interface shear behaviour: Part 1 test methods. Ground Engineering. 35(2), 35-41.

Stoll, O.W., 1971. Mechanical properties of milled refuse. Proc. of the ASCE National Water Resources Engineering Meeting, American Society of Civil Engineers, New York, pp. 11-15.

Stoltz, G., Nousheen Arif, K., Gourc, J.-P., Olivier F., Redon, E., 2009. Hydro-mechanical properties of MSW from laboratory tests following a deep drilling campaign. Proc. of the Sardinia 2009, Twelfth International Waste Management Symposium, S. Margherita di Pula, Cagliari, Italy. 10 p.

Tanchaisawat, T., 2013. Measured and Simulated Interactions between Kenaf Geogrid Limited Life Geosynthetics (LLGs) and Silty Sand Backfill. Proc. of the 18th International Conference on Soil Mechanics and Geotechnical Engineering, Paris 2013, pp. 821-824.

Tano, F., Olivier, F., 2014. Use of geosynthetics in piggy-back landfills: development of an iterative methodology for the design of the lining system over old unlined waste. Proc. of the 10th ICG 2014, September 21-25, Berlin, Germany. 8 p.

Tano, F., Olivier, F., Touze-Foltz, N., Dias, D., 2015. State-of-the-art of piggy-back landfills worldwide: comparison of containment barrier technical designs and performance analysis in terms of geosynthetics stability. Proc. of the Geosynthetics 2015, February 15-18, Portland, Oregon, USA. 11 p.

Tchobanoglous, G., Theisen, H., Vigil, S.A., 1993. Integrated Solid Waste Management: Engineering Principles and Management Issues. New York, USA. McGraw-Hill International, 2nd édition. 978 p.

Turczynski, U.,1988. Geotechnische Aspekte beim Aufbau von Mehrkomponentendeponien. Universisity of Freiberg, Germany. thesis, p.

Varga, G., 2011a. Some geotechnical aspects of bioreactor landfills. periodica polytechnica Civil Engineering. 55(1), 39-44.

Varga, G., 2012. Degradation Dependent Stability Issues of Landfills. Proc. of the Conference of Junior Researchers in Civil Engineering, pp. 267-271.

Vilar, O.M., Carvalho, M.F., 2002. Shear strength properties of municipal solid waste. Proc. of the Fourth International Conference on Environmental Geotechnics, AA Balkema, Lisse, Netherland, pp. 59-64.

Villard, P., Gourc, J.P., Feki, N., 1999. Analysis of geosynthetic lining systems (GLS) undergoing large deformations. Geotextiles and Geomembranes. 17 17-32.

Villard, P., Kotake, N., Otani, J., 2002. Modeling of reinforced soil in finite element analysis

Proc. of the 7th International conference geosynthetics, Nice, France. vol. 1, pp. 39-95.

Watts, K.S., Charles, J.A., 1990. Settlement of recently placed domestic refuse landfill. Proc. of the Institution of Civil Engineers, Part 1, London, England, pp. 971-993.

Wilson-Fahmy, R.F., Koerner, R.M., 1993. Finite element analysis of stability of cover soil on geomembran lined-slope. Proc. of the Geosynthetics 93, Vancouver, Canada.vol. 3, pp. 1425-1437.

Wu, W., Wang, X.T., Aschauer, F., 2008. Investigation on failure of a geosynthetic lined reservoir. Geotextiles and Geomembranes. 26, 363-370.

Yu, L., Batlle, F., 2011. A hybrid method for quasi-three-dimensional slope stability analysis in a municipal solid waste landfill. Waste Management. 31(12), 2484-2496.

Yuan, Z.,2002. Pullout Resistance of Geogrid in Expanded Clay Lightweight Aggregate Material. TRB2003 Session A2K07 and A2K02 - Recent Developments in Embankment Stabilization. 12 p.

Zamara, K.A., Dixon, N., Fowmes, G., Jones, D.R.V., Zhang, B., 2014. Landfill side slope lining system performance: A comparison of field measurements and numerical modelling analyses. Geotextiles and Geomembranes. 42(3), 224-235.

Zekkos, D., Bray, J.D., Kavazanjian, E.J., Matasovic, N., Rathje, E., Riemer, M., Stokoe, K.H., 2006. Unit weight of municipal solid waste. Geotechnical and geoenvironemental engineering. 132(10), 1250-1261.

Zhan, T.L.T., Chen, Y.M., Ling, W.A., 2008. Shear strength characterization of municipal solid waste at the Suzhou landfill,China. Engineering Geology. 2(97), 97–111.

Zhu, B., Gao, D., Chen, Y.-M., 2009. Geomembrane tensions and strains resulting from differential settlement around rigid circular structures. Geotextiles and Geomembranes. 27(1), 53-62.

Zwanenburg, C., Knoeff, J.G., Hounjet, M.W.A.,2007. Geotechnical characterization of waste. Proc. of the Sardinia 2007, 11th International Waste Management and Landfill Symposium, in CD Rom.